PREDICTION OF SURFACE TEXTURE PARAMETERS USING MACHINE LEARNING IN LASER SURFACE TEXTURING

By

LIHANG YANG

A thesis submitted to the

School of Graduate Studies

Rutgers, The State University of New Jersey

In partial fulfillment of the requirements

For the degree of

Master of Science

Graduate Program in Industrial and Systems Engineering

Written under the direction of

Tuğrul Özel

and approved by

____

____

____

New Brunswick, New Jersey

October 2020

ABSTRACT OF THE THESIS

Prediction of surface texture parameters using machine learning in laser surface texturing

by LIHANG YANG

Thesis Director:

Tuğrul Özel

Laser surface texturing provides several benefits such as improved tribological behavior of the surface, reduced friction, increased anti-adhesive properties and improved wettability and lubrication applications. However, surface topography or surface texture resulting from laser processing and the relation between laser texturing parameters and surface texture parameters are not well understood. Fiber lasers provide a flexible solution for texturing different materials with different surface structures.

In this thesis, experimental results from laser surface texturing of a tool steel are examined. A nanosecond fiber laser system is utilized to scan and texture the surfaces of the tool steel under a shield of an inert gas stream to prevent from oxidation. The effects of laser energy density, scan velocity, and strategy on the texture line width and resultant surface roughness have been investigated. Surface measurements in 3D are conducted using a white light interferometry based optical surface metrology system.

Surface texture parameters including arithmetic mean and root-mean squared heights of the scale-limited surface and skewness and kurtosis of the scale-limited surface can reveal the distinct effects of laser power, energy density, and scan velocity on the surface

texture parameters. Machine learning methods such as Artificial Neural Networks are utilized to generate a predictive modelling capability for the relationships between laser surface processing parameters and the resultant texture parameters on the scale-limited surfaces surveyed.

Acknowledgements

I would like to thank the members of my thesis committee; Dr. Tuğrul Özel, Dr. Hoang Pham, and Dr. Zhimin Xi, the chair of the Department of Industrial and Systems Engineering, Dr. Mohsen Jafari, the graduate program director, Dr. Myong Jeong, and staff members, Mr. Brian Alden, Ms. Laura Kasica, and Ms. Barthi Ponnuraj.

Dedication

I would like to dedicate this thesis to my family for their support and encouragement.

Table of Contents

List of Tables

List of Figures

Chapter 1

Introduction

1.1 Definitions

In the field of industrial and manufacturing engineering, *surface texture* also known as surface topography, or surface finish is the resultant micro-scale structure of a manufactured product's surfaces and is often used to describe an attribute of a product. Surface texture usually defined with three different characteristics that are surface roughness, waviness, and lay.

Lay is the direction of the predominant surface pattern, ordinarily determined by the production method used. *Surface roughness* is a measure of the total spaced surface irregularities. *Waviness* is the measure of surface irregularities with a spacing greater than that of surface roughness.

Surface measurement also known as surface metrology can be defined as measuring the topography or roughness of manufactured surfaces. Surface measurement can be performed either as two-dimensional (2D) profile measurement or three-dimensional (3D) surface areal measurement. This process can be crucial for determining a surface's suitability for a particular application. When analyzing and processing the data related to surface measurements, some terminologies are repeatedly used, such as surface form, surface finish, surface profile roughness (either as arithmetic average of surface deviations, R_a, or mean squared average of surface deviations, R_q,) and structural characterization. The ability to perform surface roughness measurements is important for maintaining component quality within predefined limits and controlling the manufacturing processes for desired performance.

2D profile measurement and analysis has been dominant in the assessment of surface texture. In modern manufacturing technology, a more precise 3D approach is required due to following reasons: (i) The surface texture is actually three-dimensional. (ii) The profile in 2D does not always represent the actual surface peaks and valleys exist on a 3D surface texture. (iii) The analysis of surface texture in 3D allows the calculation of significant new parameters for more accurate surface characterization. (4) Statistically speaking, the analysis in 3D is more precise than the analysis 2D since more data points are included and analyzed.

For these reasons, the manufactured surfaces are often characterized with 3D surface measurement data following the ISO 25178 standards for surface texture definitions [1].

These are listed as scale-limited surface texture definitions:

Sa: arithmetical mean height of the scale-limited surface.

Sq: root mean square height of the scale-limited surface.

Ssk: skewness of the scale-limited surface.

Sku: kurtosis of the scale-limited surface.

1.2 Surface Texturing and Benefits for the Manufactured Product

Surface texturing is a surface modification approach, resulting in an improvement in tribological performance such as friction and wear resistance. Surface texturing can be performed either as a protruded or recessed asperity, and it becomes more and more popular lately due to advantages in terms of micro-lubrication and ease of manufacturing [2]. Surface texturing is mainly used in improving tribological performance. The most familiar and earliest commercial application of surface texturing is that of cylinder honing. Most of ideas of adding texture on the surface of workpiece is motivated by that the surface texturing provides micro-reservoirs to enhance lubricant retention or micro-traps to capture wear debris. Usually, optimization of the texturing dimensions is done by a trial and error approach [3].

Hamilton et al. presented in 1996 [4] surface texturing in the form of micro-asperities that act as micro-hydrodynamic bearings. This idea was promoted mainly for parallel sliding, as is the case in mechanical seals [5,6].

There are numerus ways of creating surface texture, and the most advanced method used is laser surface texturing, since its flexibility and high accuracy. Other than laser surface texturing, manufacturing methods are utilized in industry for surface texturing including (i) abrasive finishing and grinding-based surface texturing, (ii) micro electric discharge machining (EDM)-based surface texturing, (iii) ion beam machining-based surface texturing and others.

Surface texturing is being used in variety of fields such as bioengineering to improve biocompatibility of metal implant surfaces, electronics to improve efficiencies of silicon wafer, automobile to reduce friction in moving mechanical components, cutting tools to reduce friction and improve lubricity.

Surface texturing is a widely used approach to improve the load capacity, wear resistance, and friction coefficient to tribological mechanical components, including sliding surfaces. Surface texture can also improve the running-in process, to smooth contact surfaces, resulting in low friction [3,4].

The effect of texturing on improving the tribological properties relies on shape, density, depth and pattern of dimples been created on the material surface. Through studies been done by different groups, it becomes a fact that Micro-textured surfaces can improve the tribological performance between parts in contact, by modifying the stress distribution, improving the friction coefficient, and reducing the amount of heat transferred between the parts. The micro-cavities which known as dimples acting as lubricant reservoirs, they provide lift effect by generating hydrodynamic pressure to reduce the surface contact between two parts, such as reducing the friction between piston and engine block or between gears in a transmission.

1.3 Motivation and Research Objective

The main motivation for this thesis is to achieve higher sustainability of metal surface texturing process by using fiber laser, in terms of reducing friction, improve tribological behavior, improve wear-resistance. Also, by importing in-situ process monitoring technique, the stability of laser texturing process hopes to be improved.

Statistical or intelligent process models should be developed to predict the behavior of laser processing.

The main focus of this research is to explore the combinations of fiber laser processing parameters which may create fine finished micro-textured surfaces. Those combinations of laser parameters which lead to process out of control will affect the stability of texturing via laser ablation by having under-ablated or over-ablated sections on the work piece surface, compromise the surface morphology, eventually cause surface irregularities.

This proposed research will seek answers to the following questions. How can one understand how the laser parameters affect the formation of textured surfaces? How would the same surface textured workpieces that were produced by different laser parameters perform under the same loading conditions? How does adding micro-texture with different laser parameters contribute to the tribological performance? What is the optimum combination of laser texturing parameters?

Chapter 2

Laser Surface Texturing

Surface texturing are commonly used on parts and components in contacted with each other such as bearings, pistons, and cylinders. It is also used in structuring cutting tools geometry and surfaces. During the manufacturing process of those workpieces, a same property is shared, that they all made from high strength metal materials (e.g. tungsten carbide, ceramics) which are difficult to be machined. But due to the recent development of advanced manufacturing technologies, it is possible to accurately fabricate different type of surface morphologies on the workpiece, and many manufacturers take advantages of such technologies to advance their products' performances. Currently following advanced manufacturing technologies are widely adopted by manufactures, abrasive finishing and grinding based surface texturing, micro EDM based surface texturing, and laser processing-based surface manufacturing. In this thesis, the focus will be on laser processing based advanced manufacturing of surface textures. The behavior of laser processing and ablation is known as difficult to understand, and there are more than hundred parameters can affect the overall quality of the textured workpieces, so it is necessary to introduce machine learning and statistical learning during to improvement of such processes. A model should also be developed to estimate and predict the behavior of laser surface texturing process.

2.1 Laser Surface Texturing for Friction Reduction

Laser surface texturing (LST) involves making patterns on surfaces to improve properties and performance of engineering applications [7, 8]. Etsion [7] states that laser processing became the most popular method among various other texturing methods because it offers the most promising design flexibility and allows shorter processing times since it is extremely fast and direct not requiring tooling. It is an advanced, sustainable, environmentally friendly production method that gives the best shape and size an end user expects [8].

It is reported that tribology related improvements at interface contacts can be achieved such as reduced wear rates, forces and load, improved lubrication [9] and reduced friction coefficients [10]. Laser texturing provides distinct patterns on surfaces at micro scales in the form of very fine detailed geometrical features such as grooves, dimples, cross-patterns with high depth resolution. As mentioned, it allows the creation of textures that change the functional properties of surfaces, improved anti-adhesive behavior, reduced friction or altered optical properties.

An example of a dimple texture applied to a drilling tool's surface is shown in Figure 1. The curved flute surface of a drill is machined with a texture consisting of oblong shaped dimples with a non-symmetrical cross section.

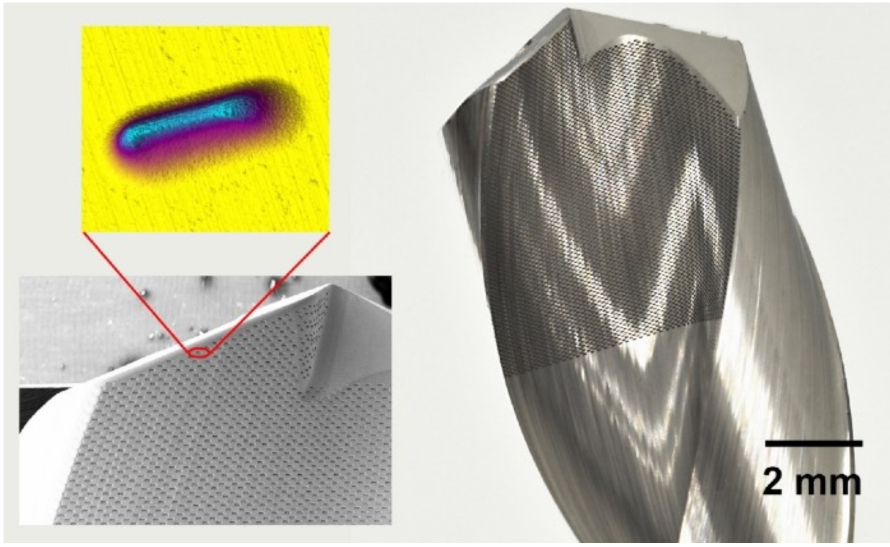

Figure 1. LST regular micro-surface structure in the form of micro-dimples (Courtesy of Lightmotif company).

In a tribology study, the micro-dimples were created on the surfaces of stationary and rotating ring walls by using LST. A trial-and-error approach was adopted. The result of the experiment was as expected from theory. Micro-dimples functioned as micro-traps for wear particles or micro-reservoirs for lubricant retention. However, in other cases, where the micro-dimples functioned as micro-hydrodynamic bearing, the effects was not clear and it was recommend further study to be performed to investigate and optimize the LST parameters for the best tribological performance (see Fig. 2).

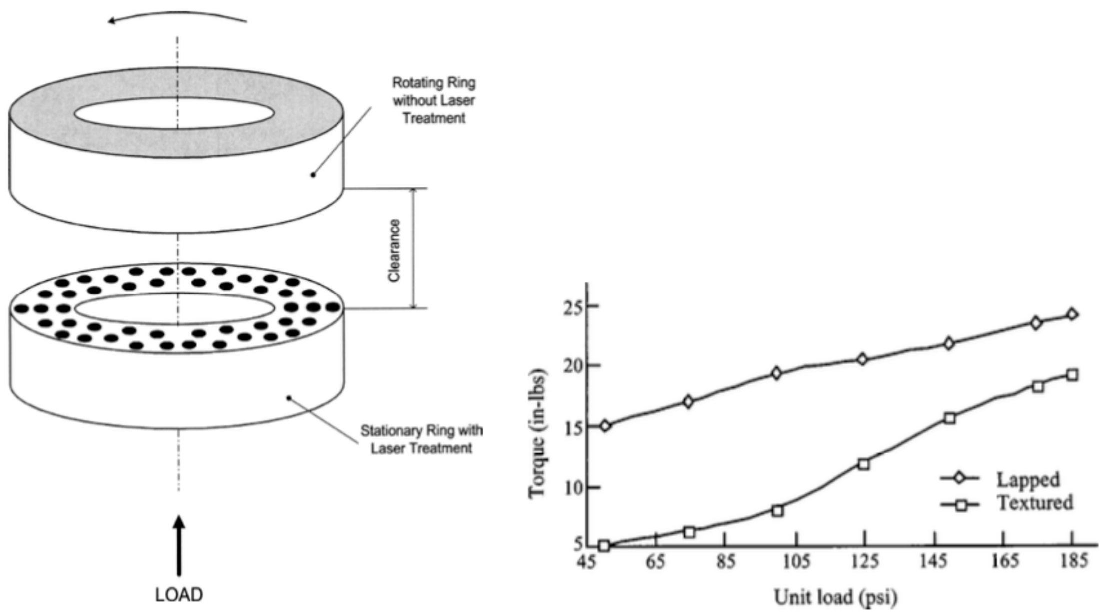

(a) (b)

Figure 2. Seal model and mode of operation (a) and comparison of the friction torque for textured and nontextured surfaces (b).

Based on the experiment designed and performed by the authors, the increase in tribological performance was clear as expected. Testing of the sealing prototype in water showed dramatic reduction of up to 65% in friction torque. The reduction in friction torque is gradually disappeared at higher sealing pressures, corresponding to higher unit loads. The solution for this phenomenon was seen as applying higher density LST over a portion of the sealing wall adjacent to the high-pressure side and leaving the remaining portion as non-textured. The result in the corresponding friction torque of the textured seal at higher pressure was unbelievably small, and a reduction in friction of more than 90% was achieved.

2.2 Laser Surface Texturing for Changing Surface Wettability

The laser surface texturing process can be applied on any material and can be used for texturing complex curved surfaces as well. Several different properties for a large field of applications and in different industries can be provided with fine textured surfaces. For example, micro-texturing has created surfaces with tailorable chemical and wetting properties for improved biocompatibility or biological reaction in biomedical applications [11,12]. Therefore, laser surface texturing at micro scale offers several tribological and biological benefits while retaining the main functionality of the structure.

Nanosecond pulsed laser processing was utilized to reduces the wettability change of a copper surface from a hydrophilic surface to a superhydrophobic surface using additional low-temperature annealing [13].

To create a superhydrophobic surface on metals, laser beam machining and chemical coating have been widely utilized, some researchers tried to use only laser machining with our extra coating for easy fabrication and removal of unwanted properties of the coating layer. However, this approach resulted in a very long time for hydrophilic surface to change to superhydrophobic. Chun et al. [13] stated that by using nanosecond laser surface texturing, it will take 30 days for aluminum to achieve a nearly superhydrophobic or superhydrophobic surface. By using femtosecond laser processing, it requires also 30 days for stainless steel 304L surface to fully change. Also 11-12 days for copper/brass by a nanosecond laser to achieve a nearly superhydrophobic or superhydrophobic surface [8-12].

This paper conducted a research that after laser machining, by utilizing the laser surface texturing techniques along with low temperature annealing, material achieved superhydrophobic within hours, and the time was reduced even more with the use of ethanol [13].

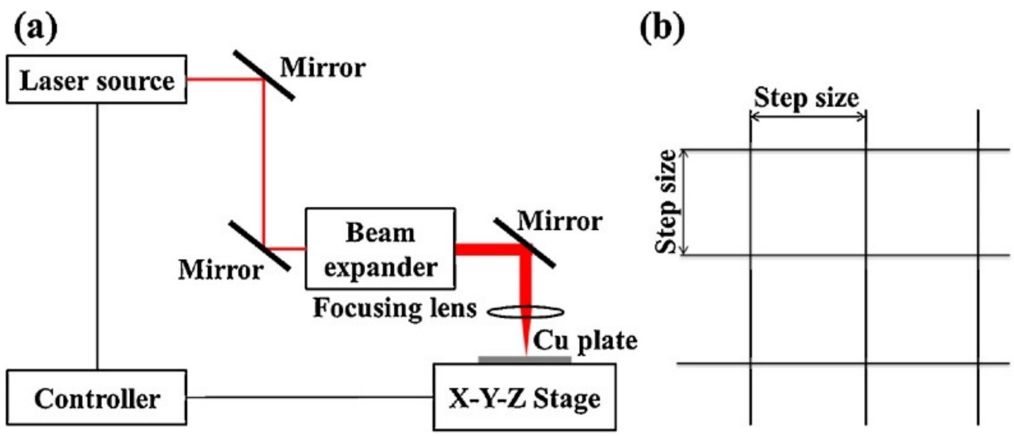

Figure 3: Schematics of the laser beam machining system (a) and (b) beam path design [13].

In experiment performed in this article, a Q-switched Nd: YAG 355-nm UV nanosecond pulsed laser was utilized since this is the most common and widely accepted setup in the industry (see Figure 3). Pure copper plate with 2 mm thickness was used as a substrate, laser beam machining was carried out with a grid pattern, which showed isotropic superhydrophobic properties in all directions with trapped air. Adding ethanol on the laser textured surface with low temperature annellation will acceleration the reaction since copper is stable with ethanol and organic materials can enhance superhydrophilicity of laser textured metals (see Figures 4, 5, 6).

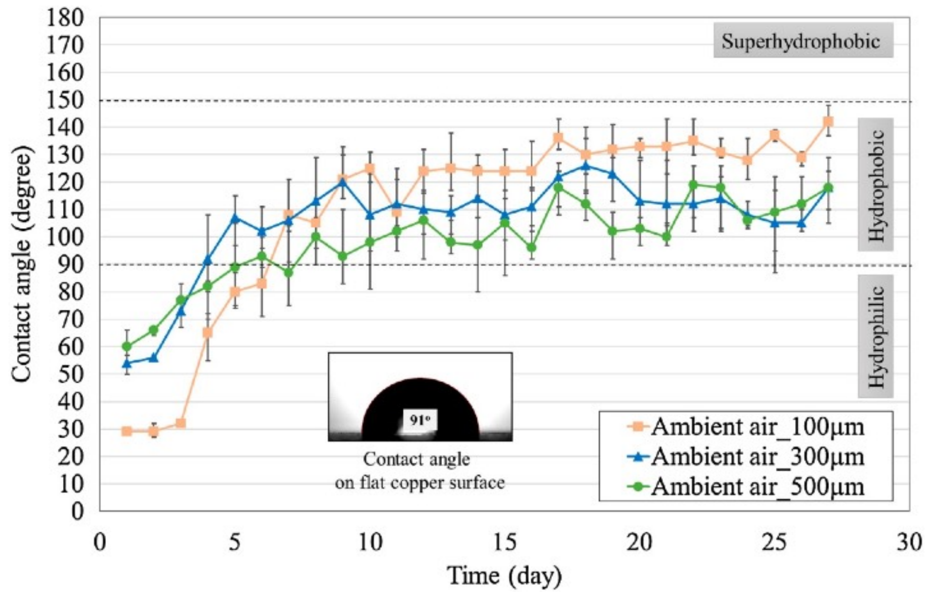

Figure 4. Measure of water droplet contact angle of samples exposed to ambient air [13].

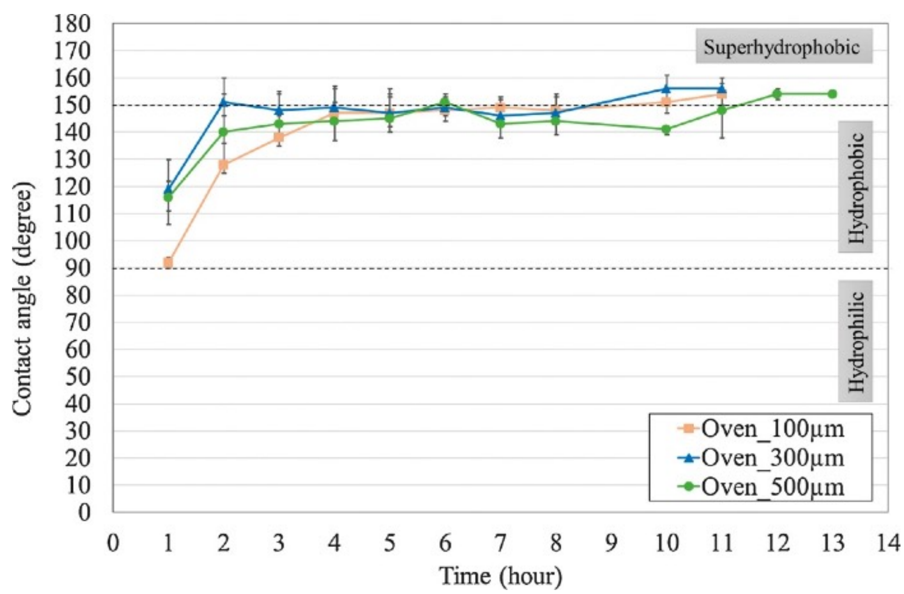

Figure 5. Measure of water droplet contact angle of samples with low-temp annealing without ethanol [13].

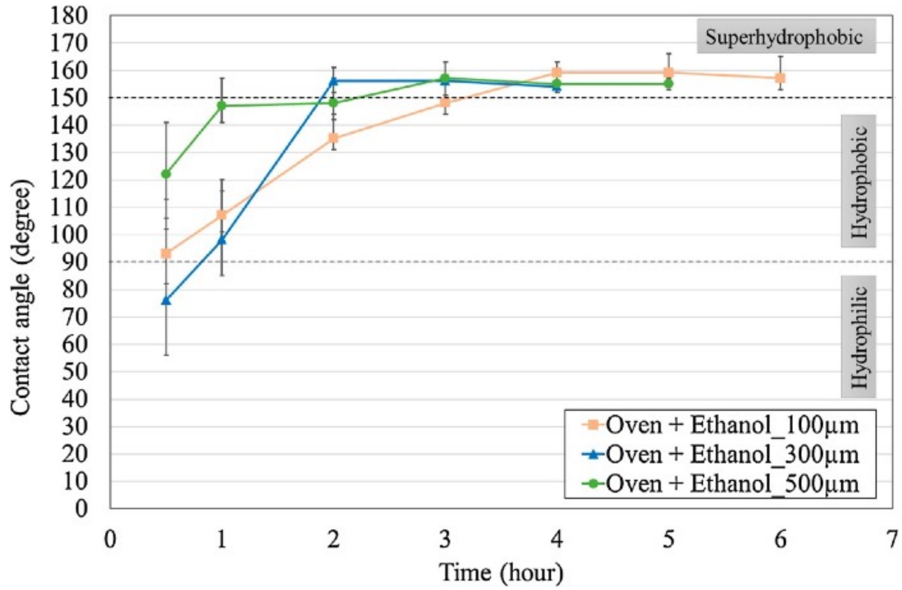

Figure 6. Measure of water droplet contact angle of samples with low-temp annealing with ethanol [13].

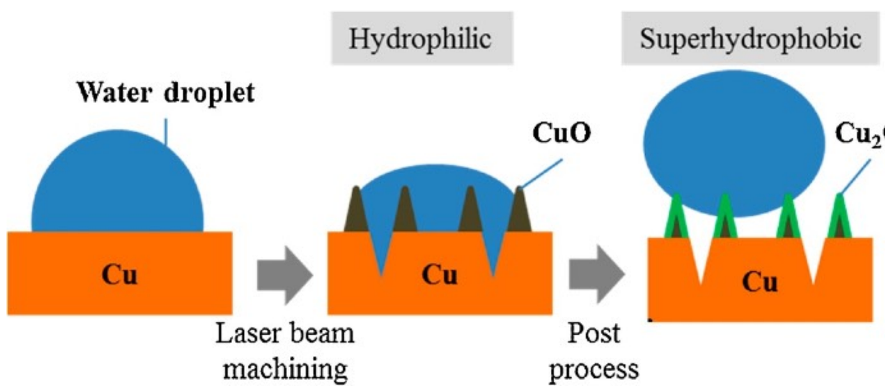

Figure 7. Schematic image of mechanism for superhydrophobic to superhydrophobic surfaces with laser beam machining and post process [13].

The significant time change is explained in this article, that due to laser texturing, the molten copper becomes a CuO structure, which is hydrophilic. Then the top layer of CuO rapidly becomes Cu_2O which is a hydrophobic material, a hydrophobic material with post process and a partially wetted state with grid patterned burrs were necessary for a superhydrophobic surface (see Fig. 7) [13].

2.3 Laser Surface Texturing for Cutting Tool Tribological Performance

Recently, laser surface texturing gained attention due to the improvement on tribological performance of cutting tool surface. But the effective texture patterns and dimensions on a tool surface still need to be investigated and studied through trial-and-error method.

For machining applications, cutting tools having micro-textured surfaces have been also developed by using laser surface texturing. These are developed on high speed steel for cutting aluminum [14], as well as on advanced tool materials such as cemented carbide for cutting steel [15] and polycrystalline cubic boron nitride or diamond for machining difficult-to-cut materials; laser textured dimples tested on cemented carbide tools [16], surface texturing applied on cubic boron nitride for anti-adhesion in high speed cutting of Inconel 625 alloy [17], and micro/nano-textures created on diamond tools for higher wear resistant cutting [18].

There are often two different types of surface texture patterns are applied on tool surface; groove-shaped and dimple-shaped textures. Sugihara & Enomoto [16] focused on dimple-shaped textured surface with different dimensions and arrays, generated on the tool rake face. They evaluated the wear resistance and cutting forces of the developed tools with a series of face milling experiments on medium carbon steel under wet and dry cutting conditions [16]. Laser surface textures were fabricated using femtosecond ytterbium-doped Yb:KGW laser with a wavelength of 515 nm, a pulse width 190 fs on the rake face of the WC-Co cemented carbide cutting tool with a 100 µm wide chamfer (see Fig. 8). A constant depth of D_{dep} = 5 µm, a distance from chamfer of E_w= 30 µm, and dimple spacing of D_{in}= 75 µm were applied to all milling inserts. Dimple diameters were varied as D_{dia} = 50, 30, 70 µm for linear tool designs DT-01, DT-03, DT-05 and for zigzag tool designs DT-02, DT04, DT06 respectively. Texture pattern was further altered by changing dimple spacing to D_{in} = 90 µm for linear tool designs DT-07, DT-09 and for zigzag tool designs DT-08, DT10 respectively (see Fig. 8 for micro-texture parameters).

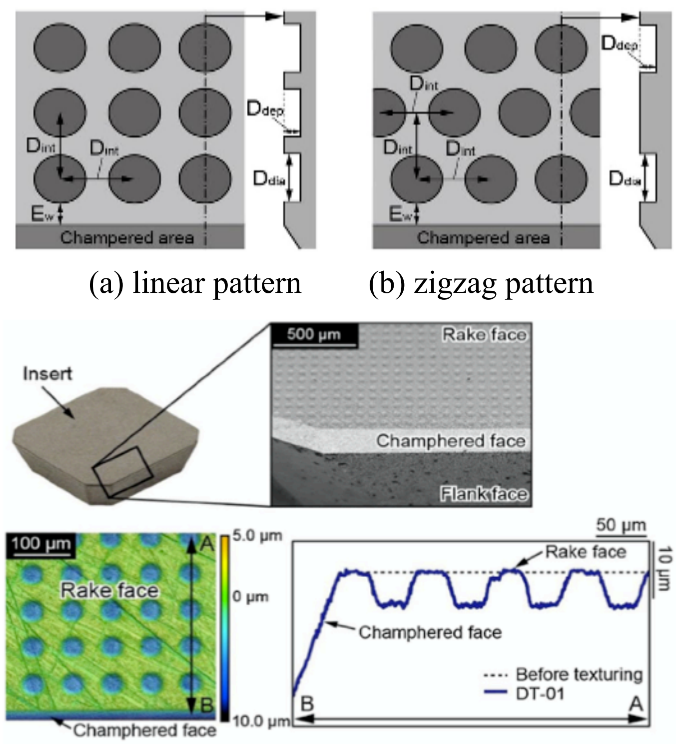

Figure 8. A milling insert and its rake face micro-textured with micro-dimples [16].

The cutting experiments were conducted on medium carbon steel using a vertical machining center by using a cutting speed of v_c = 200 m/min, and a feed rare of f = 0.2mm/tooth as shown in Fig. 9 [16] under both dry and lubricated cutting conditions.

The crater wear on the rake face of the milling tool inserts were inspected. The result of the performance for laser textured tool was as expected no matter what the cutting condition was. Especially for tools DT-05 and DT-06 which share the same geometrical parameter of dimples, but a different alignment performed better than other combinations in both cutting condition.

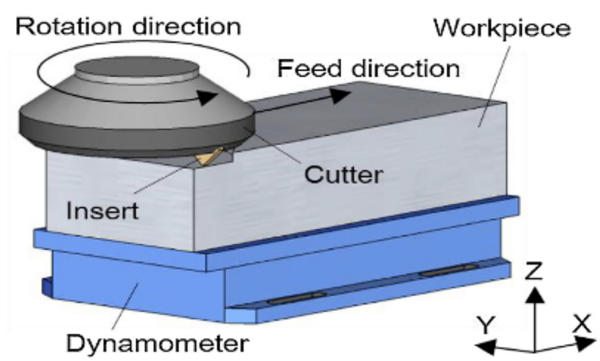

Figure 9. Schematic image of milling experimental setup [16].

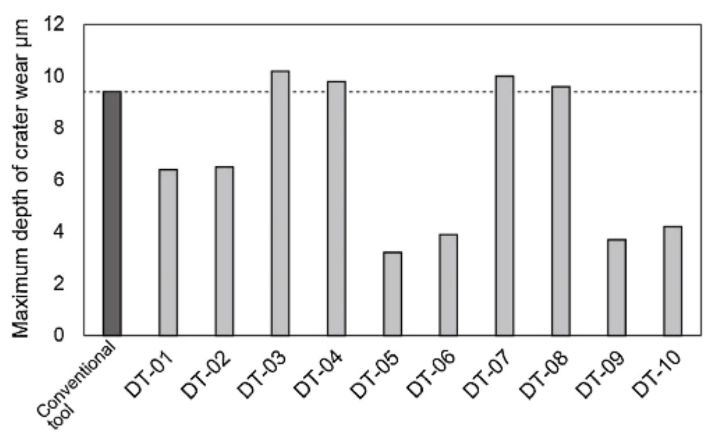

Figure 10. Crater wear of textured tools under the wet cutting condition.

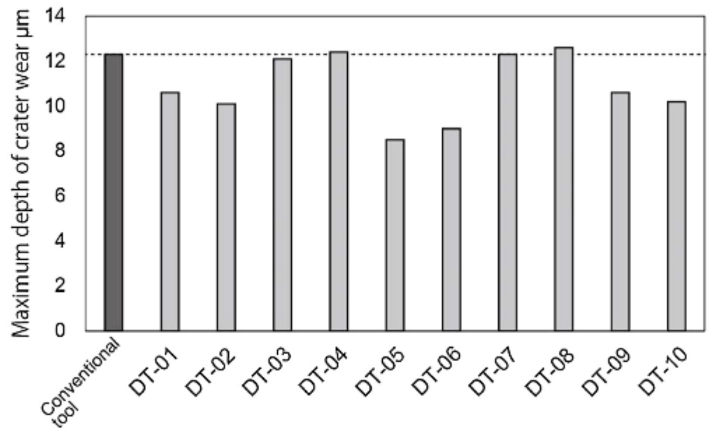

Figure 11. Crater wear of textured tools under the dry cutting condition.

In addition, Sugihara & Enomoto [16] fabricated cutting tools with micro-grooved textures for comparison against the cutting tools with micro-dimpled textures. Figure 12 shows their design on micro-grooved cutting tool rake face and the measured micro-groove geometry. They performed experiments to compare micro-dimpled tools against the micro-grooved tool under dry, paste, and wet cutting conditions (see Fig. 13).

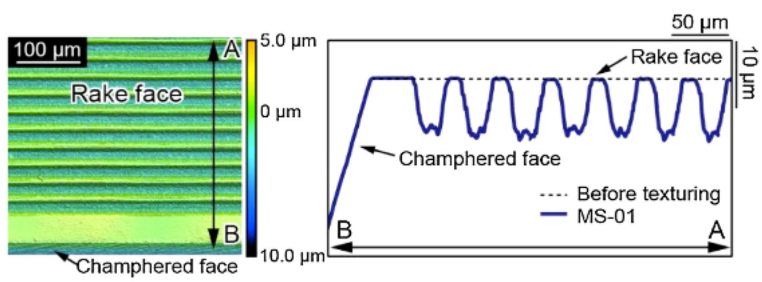

Figure 12. Developed cutting tool with micro-groove textured rake face (MS-01).

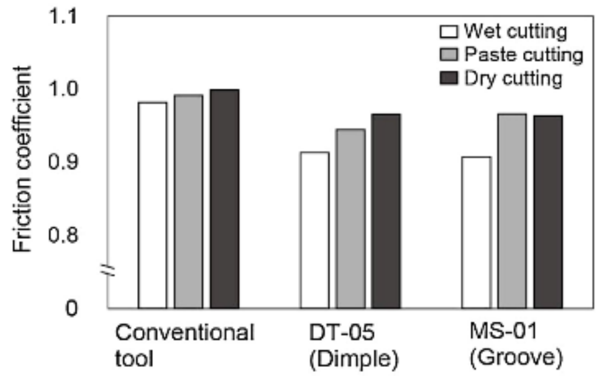

Figure 13. Friction coefficient at tool-chip interface under different cutting conditions [16].

From the experimental comparison, Sugihara & Enomoto [16] concluded that "open shape" texture in the form of micro-grooves performed better results in crater wear and friction coefficient when compared with conventional cutting tools. Furthermore, the "close shape" structure in the form of micro-dimple textures performed even better than micro-dimpled texture when cutting steel workpieces. They also noted that when cutting low melting point materials such as titanium alloys, both textured cutting tools showed much less adhesion behavior compared to the conventional cutting tools.

The explanation behind this observation is very straight forward. In surface textured cutting tools, the micro-texture pattern, especially close shaped texture, act like micro-reservoirs for the cutting fluid and micro-traps for wear debris. Therefore, under both wet and dry cutting conditions, textured tools performed a lot better than the conventional tool.

2.4 Laser Surface Texturing for Tribology Enhancement in Drilling of Titanium Alloys

The work of Sugihara & Enomoto [16] provided sufficient evidence that laser texturing can reduce the friction between workpiece and cutting tools and improve the tribological performance by significant amount. Currently, in manufacturing, cutting titanium alloys such as Ti-6Al-4V still remains challenging, since metals like titanium has much lower thermal conductivity compared with steel, so build-up edges always is one of the main affections which compromise the quality of manufactured workpieces.

Niketh & Samuel [19] utilized laser surface texturing technique, adding textures on both the flute and margin side of the drilling tools with an objective to minimize the cutting forces by reducing the sliding friction at the tool-chip and tool-work piece interfaces as shown in Figs. 14 and 15.

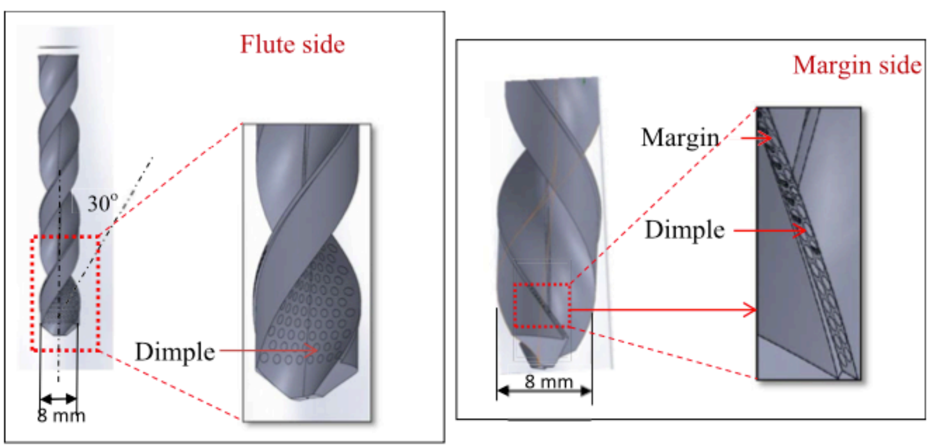

Figure 14. CAD drawing of micro textures at the flute and margin side [19].

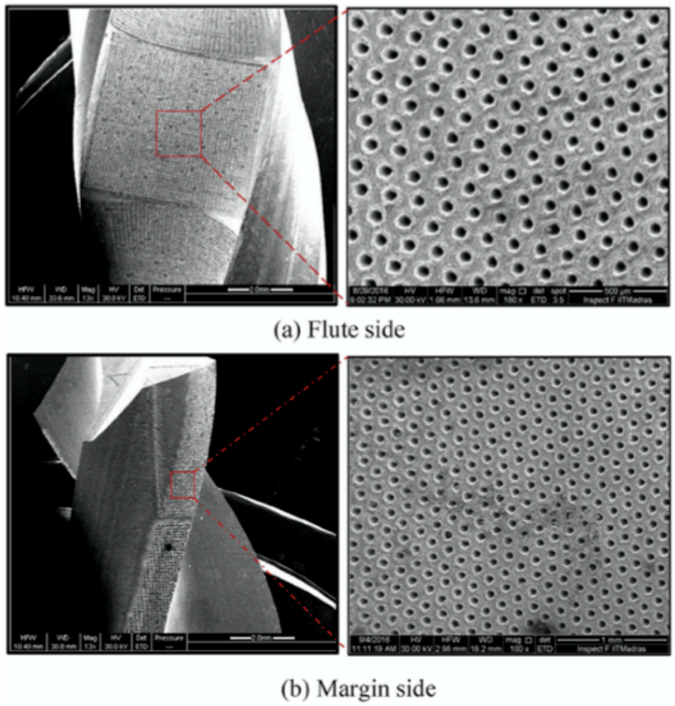

Figure 15. SEM image of micro textures at the flute and margin side [19].

The micro-dimples fabricated were evaluated by using optical imaging and 3D aerial texture measurements as given in Fig. 16. Micro-textured drilling tool surfaces were patterned with micro-dimples with slightly varying dimensional accuracy as shown in depth profile of the tool surface with micro-dimples.

Drilling process experiments were carried out on Ti-6Al-4V work material under dry cutting conditions by using three different combinations of carbide drilling tools; i) flute textured only, ii) margin textured only, and iii) non-textured. The machine tool provided a spindle speed range up to 6000 rev/min and a maximum traverse range of 350 mm (x-axis), 300 mm (y-axis), 300 mm (z-axis). A six-component dynamometer with eightchannel charge amplifier was used for recording the thrust force and torque generated during drilling [19]. The schematics of the forces in drilling process are shown in Fig.17.

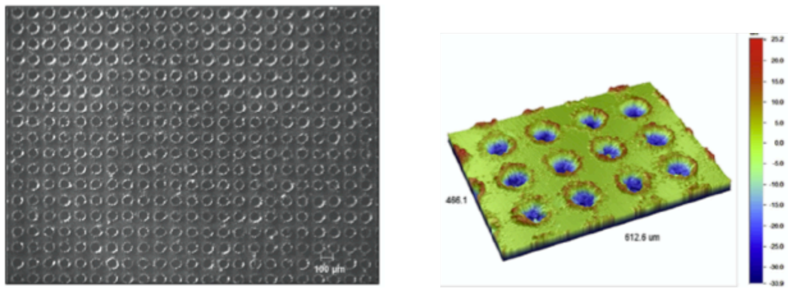

(a) optical image of micro-dimples (b) 3D measured aerial texture

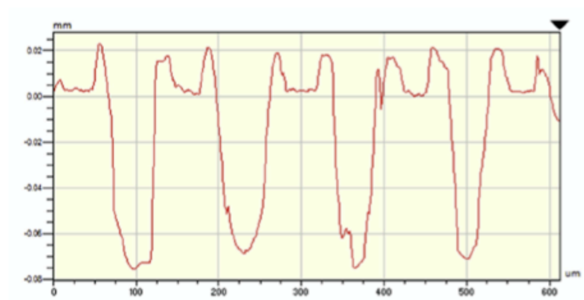

(c) Depth profile of the micro-dimples

Figure 16. Characterization of drilling tool surface with micro-dimples [19].

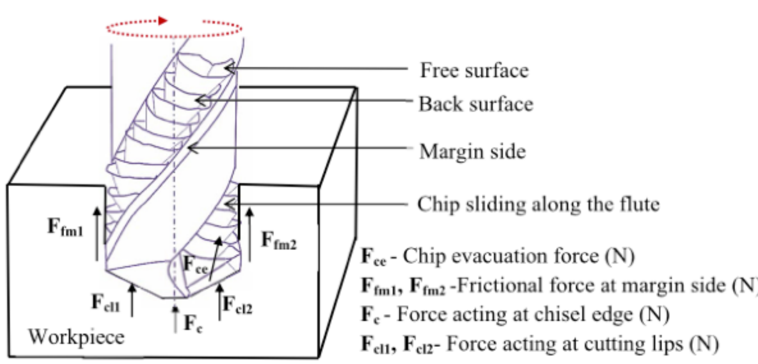

Figure 17. Schematics of the drilling process [19].

The friction results for textured surfaces was found to be favorable with lower friction coefficients as given in Fig. 18. The results on measured thrust force and torque during drilling also revealed the lowered force and torque when using textured drill tool (see Fig. 19).

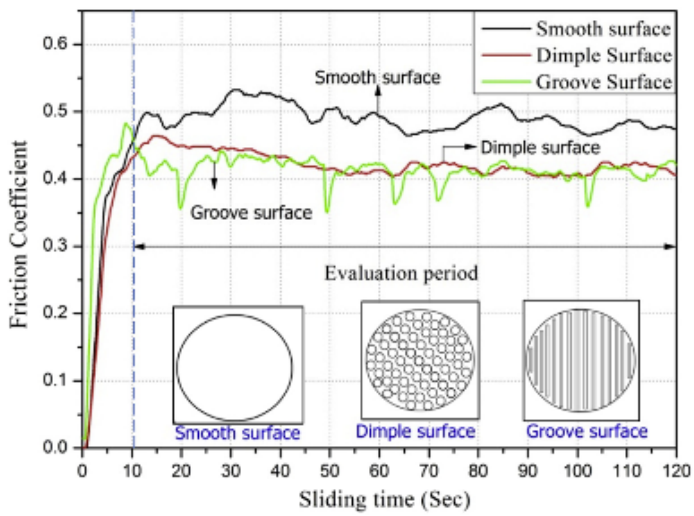

Figure 18. Variation of friction coefficient with sliding time for textured and non-textured surfaces [19].

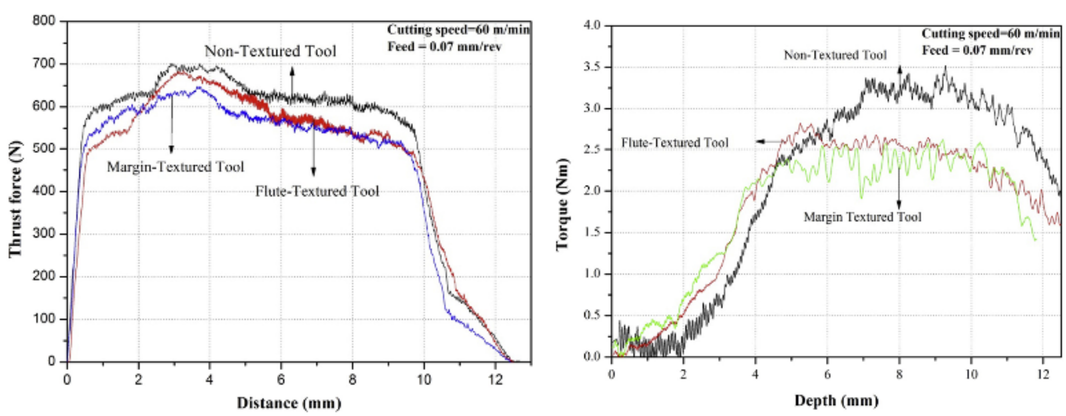

Figure 19. Comparison of the thrust force (a) and torque (b) during drilling [19].

By analyzing the force data and observation the chip morphology, the authors found out that there is 16.33% reduction in friction coefficient while using micro-grooved surface and 14.29% reduction in case of micro-dimpled surfaces. A net reduction of 10.68% in thrust force and 12.33% in torque was reported in the case of margin textured tool even at a higher cutting speed of 60 m/min and a feed of 0.07 mm/rev [19].

Therefore the conclusion is very clear that micro dimples at the margin were effective in reducing the sliding friction between drill head and workpiece, and flute textured minimizes the contact length of chip clogging phenomenon leading to a lower chip evacuation force [19].

Chapter 3

Nanosecond Laser Surface Texturing Experiments

3.1 Laser Processing Characteristics and Parameters

In recent studies, it is shown that laser surface texturing with picosecond (ps) fiber lasers on tool steels can be performed competitively with adequate results, efficient pulse repetition rates and processing times [20]. The laser energy density can be controlled by modulating the laser power and scan velocity to obtain an ideal texture or pattern generation. Depending on the laser power and scan strategy, microstructures in the order of a few micrometers (µm) along with macrostructures over millimeter (mm) topographies can be generated.

In general, laser parameters that are related to physical characteristics include power, wavelength, pulse duration, pulse repetition rate, and focused spot size as listed in Table 1.

Table 1. Laser characteristics.

Characteristic	Symbol	Unit
Laser power	P	[W]
Laser wavelength	λ	[nm]
Laser pulse energy	E	[mJ]
Pulse duration	τ	[s]
Laser spot size	d_0	[mm]
Laser energy density	Φ	[J mm^{-2}]

For instance, laser texturing using picosecond solid state Nd: Vanadate (Nd: YVO 4) (τ= 10 ps, λ= 1064 nm, PRR= 5 kHz) for micro-dimple fabrication on titanium alloy Ti-6Al-4V and aluminium alloy AA2024 was performed [21]. Dimpled surface textures were created with laser ablation at pulse energies in the range of Φ =1 μJ and Φ = 20 μJ and by applying in the range of 10 to 200 pulses per dimple.

On the other hand, laser surface processing involves a set of parameters that are programmable by using numerical programming of the positioning stage that moves the workpiece as listed in Table 2.

Finally, the micro-texture lines are fabricated through laser ablation that includes the following dimensional characteristics (see Table 2).

Therefore, this study aims to investigate the relation between the nanosecond fiber laser processing parameters (laser power, scan velocity) and the resultant micro-texture line width and surface texture parameters for the AISI D2 tool steel workpiece.

Table 2. Laser surface processing and texture line dimensional parameters.

Parameter	Symbol	Unit
Pitch between laser tracks	p	[mm]
Scan velocity	v_s	[mm s^{-1}]
Texture line length	l_l	[mm]
Texture line width	w_l	[mm]

3.1 Laser Surface Texturing of AISI D2 Steel

In this thesis study, an experimental system for laser surface texturing was developed in which a ytterbium pulsed fiber laser (YLP-V2-1-100-50-50) from IPG photonics that operates at 1064 nm wavelength, 50 W maximum power, 100×10^{-9} s pulse duration, and 20×10^{3} s^{-1} nominal pulse repetition rate was employed. The fiber laser was coupled to a 1064 nm high power focusing objective (Thorlabs LMH-5x-1064). The focusing lens provided a focus length of 35 mm. The collimated beam diameter is 5.9 mm. The beam quality factor $M^2 < 2$. The focused beam diameter was measured to be 0.150 mm ± 10 μm. The experimental laser surface texturing apparatus used in this investigative study is shown in Fig. 20. The laser beam delivery optics is used to focus the beam on the top surface of the work piece. The fiber laser collimator and the optics were mounted onto the Z-axis motion stage for simplicity in adjusting and controlling the focal position. This was used for controlling the motion of laser beam. Since the beam delivery optics can introduce power losses to the laser surface texturing system, a power meter was used to measure laser power. A two-axis XY positioning system (Aerotech Model ATS100-100-20P) was used to control the position of the workpiece sample.

A flow chamber was designed for focus beam coupling with Argon gas supply. The design requirements that were considered are that the flow chamber shall clamp to the fiber laser and house the focusing beam concentrically beneath the laser's collimated beam, it would allow the focused beam to reach to the workpiece surface that is 35 mm away from the objective lens. Therefore, a flow chamber design was created for shielding gas without any leaks for contaminated air to enter as shown in Fig. 21. A standard flow rate of 0.567 m3 hr -1 Argon shielding gas O-2 (98% argon/ 2% oxygen) supply was used as sufficient enough to shield the laser processed steel surface from oxidation.

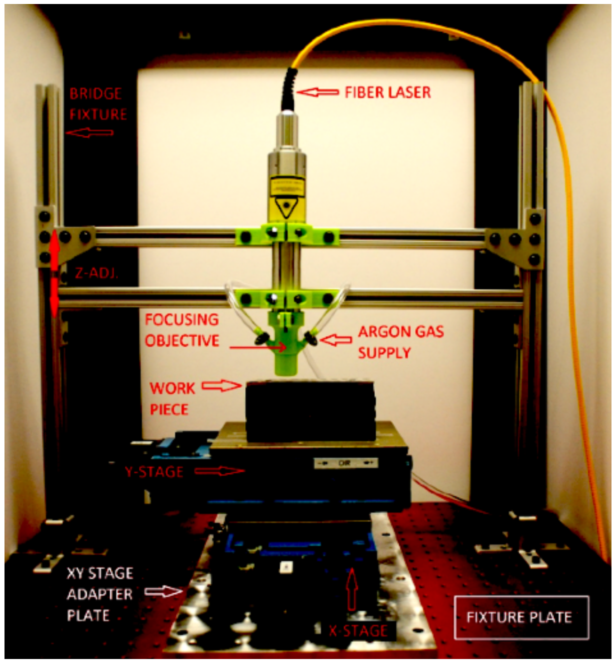

Figure 20. The experimental laser surface texturing system used in this study.

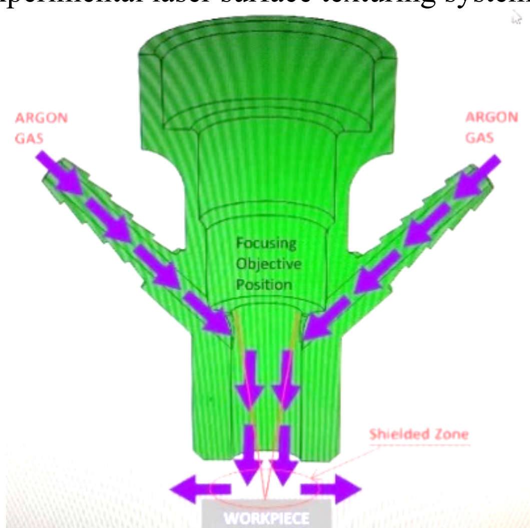

Figure 21. The flow chamber designed for Argon gas shielding.

AISI D2 tool steel is a high carbon, high chromium cold-work steel and has good corrosion resistance. The chemical composition is given in Table 3. Its yield strength and Young's modulus are 650 MPa and 209.9 GPa respectively. It also possesses better than average wear resistance and retains its hardness up to 425 °C. In this study, the workpiece specimen is selected as an AISI D2 tool steel plate with a thickness of 3.175 mm that is ground to a fine surface finish with arithmetic surface roughness of Ra = 0.06 µm. The hardness of the specimen is measured as 61.5 ± 0.5 HRC before laser surface texturing.

Table 3. Nominal chemical composition of AISI D2 tool steel.

Element	C	Cr	Mo	Si	Mn	P	S	V
wt. %	1.5	11.0	0.90	0.30	0.45	0.030	0.030	1.0

Micro-textures were fabricated on the ASI D2 tool steel surface by a fiber laser system that operates with a constant pulse duration of 100×10^{-9} s, a constant pulse energy of E = 0.1 mJ, and a constant wavelength of λ = 1064 nm. The laser power can be regulated by increasing the pulse repetition rate between PRR = 10 kHz and 50 kHz as given in Eq. (1).

$$P = E \bullet PRR \tag{1}$$

Micro-grooves perpendicular to the direction of the texture were fabricated on the surface through ablating AISI D2 tool steel material by fiber laser again as shown in Fig. 22. The laser trajectory is controlled by the computer controlled 2-axis XY positioning stage to move the workpiece a certain distance in the X direction, while the subsequent laser beam is at a hatch distance of p from the last laser line in the Y direction. The initial laser surface texturing parameters were listed as; a processing area of A = 2 mm · 8 mm, a constant maximum pulse energy of $E = 0.1$ mJ, a scan velocity of $v_s = 0.8$ mm.s^{-1}, a pulse repetition rate of $PRR = 50$ kHz and a hatch spacing of $p = 0.2$ mm.

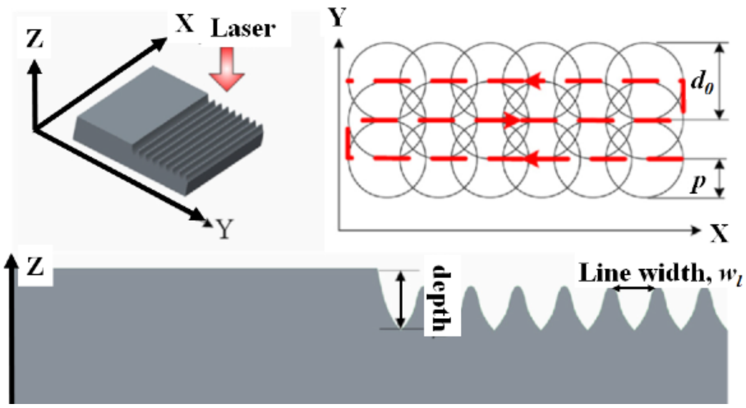

Figure 22. The processing path for the laser beam in laser surface texture.

The energy density provided during laser surface texturing is estimated using the laser power, P, and scan velocity, v_s, and the focused laser beam diameter d_0 as given in Eq. (2).

$$\Phi = \frac{P}{v_s d_0} \qquad (2)$$

The flow chamber coupling design (see Fig. 22) integrated optical components and also channeled the Argon gas in order to shield the processed steel's surface while focused laser beam processes it for ablation. Scan velocities of $v_s = 0.625$ mm s^{-1}, 0.833 mm s^{-1}, and 1.538 mm s^{-1} have been tested. The detailed fiber laser surface texturing parameters are given in Table 4.

Table 4. Laser surface texturing parameters.

Parameter	Value	Unit
Laser power, *P*	20, 30, 40, 50	[W]
Pulsed repletion rate, *PRR*	10, 20, 30, 50	[kHz]
Scan velocity, v_s	0.625, 0.833, 1.538	[mm s^{-1}]
Pitch between laser tracks, *p*	0.1, 0.2	[mm]
Trajectory	Linear, double, cross	[-]

Nanosecond fiber laser processing of AISI D2 tool steel for surface texturing is achieved by continuously irradiating the sample with the focused laser beam in order to ablate a thin surface of the steel substrate thermally through melt formation. Therefore, the ablated steel vaporizes initially creating small valleys, and when solidifying, the surface tension smooths the workpiece surface, hence reducing the roughness forming the texture.

The optical configuration and the control of the laser power allow the accurate determination of the surface texture modification. With low or modest laser energy density that irradiates the workpiece, the tool steel substrate reaches its melting temperature, whereas at high laser energy density vaporization temperature is reached. These two different temperature profiles will lead to a successful texturing without melting a wider area.

3.2 Line-to-line and Pulse-to pulse Overlapping

Laser trajectory produces a path with a width defined by the diameter of the laser beam focal spot formed by the laser and focal objective. The amount of overlap produced by parallel laser trajectories is the pitch distance between parallel lines. The finished area on the surface is the result of multiple overlapping trajectories. The trajectory line overlap percentage (LO%) is introduced as a parameter that describes the impact of overlapping trajectories on the change in surface texture parameters and is defined as in Eq. (3),

$$LO\% = (1 - \frac{p}{d_0}) \times 100 \qquad (3)$$

where p is the pitch distance (mm) between trajectory lines, d_0 is the laser beam spot size (mm) formed by the laser beam and focal objective. This was kept constant as $LO\%$ = 33.33% in study and its effect is not investigated yet. Another parameter, a pulse overlapping factor, is also defined as it ranges between 99.95% and 99.99% for v_s = 1.538 mm s^{-1}, PRR = 20 kHz, d_0 = 0.15 mm, P = 25 W, achieving a fluence of $\Phi_{99.95\%}$ and v_s = 0.625 mm s^{-1}, PRR = 50×10^3 s^{-1}, d_0 = 0.15 mm, achieving a fluence of $\Phi_{99.95\%} = 213.3\ J.mm^{-2}$ respectively using the expression given in Eq. (4).

$$PO\% = (1 - \frac{v_s}{d_0\, PRR}) \times 100 \qquad (4)$$

By using linear, double and cross pattern trajectories for laser processing, texture patterns such as line, grid, and chaotic patterns have been obtained (Fig. 23) and the lines with micro-grooves have been further analyzed to understand the effect of laser parameters on the resultant textured surface.

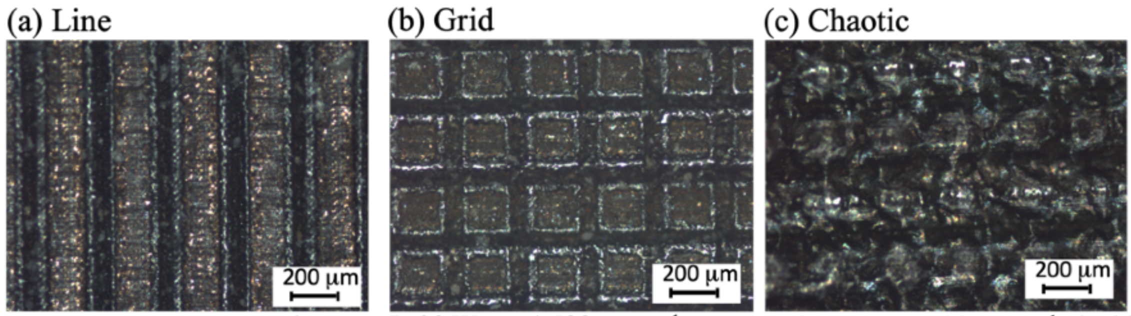

P = 20 W, v_s= 1.538 mm.s^{-1}, linear P=20 W, v_s= 1.538 mm. s^{-1}, cross P=35 W, v_s= 1.538 mm. s^{-1}, double

Figure 23. Texture morphology to improve adhesion strength of AISI D2 steel.

3.4 Surface Areal Texture Measurements

The surface areal topography was measured after laser texturing by using a Polytec TopMap E42405 (by Ploytec GmbH) white light interferometry based optical surface metrology system with a 1.45 nm vertical resolution [22]. These textured surfaces have been characterized with the arithmetical mean height of the scale-limited surface *Sa*, the root mean square height of the scale-limited surface *Sq* (standard filtering conditions), and *Ssk* and *Sku*, skewness and kurtosis of the scale-limited surface respectively according to ISO 25178-2 [23] with the optical metrology system.

These measured surface areal height maps of textured surfaces in colored scale are given in Figs. 24, 25, 26 for the texture produced with single, double, and triple pass scan strategies respectively. During measurements, scale-limited (SL) surfaces were obtained by applying form removal F-operator (fitting with nominal shape), short-scale component removal with S- filtering, and long-scale component removal L- filtering using the default settings of ISO 25178-3 [24] in the instrument software of the PolyTec white light interferometry based measurement system. At first, levelling and filtering was performed.

A Gaussian regression L-filter nesting index of 8.0 mm and an S-filter nesting index of 0.025 mm, per ISO 25178-3, were applied to each surface. A linear regression approach, S-filter gaussian high pass with 8.0 mm, gaussian low pass with 0.05 mm and then parameter calculation by applying gaussian filter with a nesting index of 0.8 mm was performed.

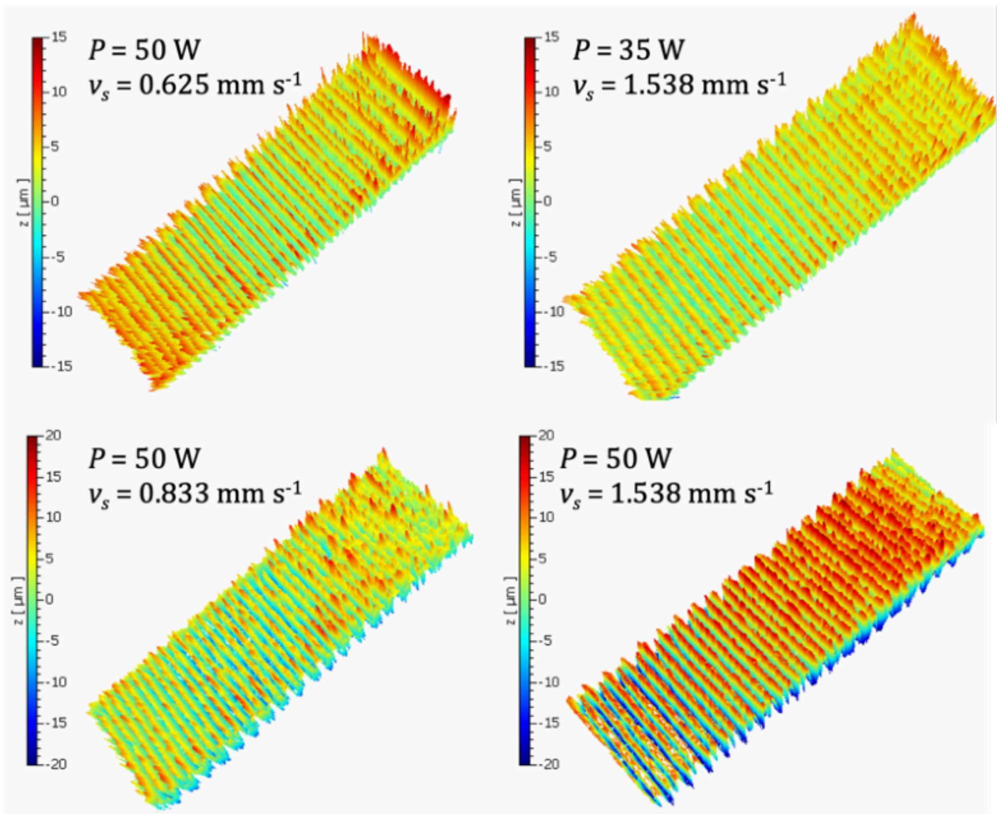

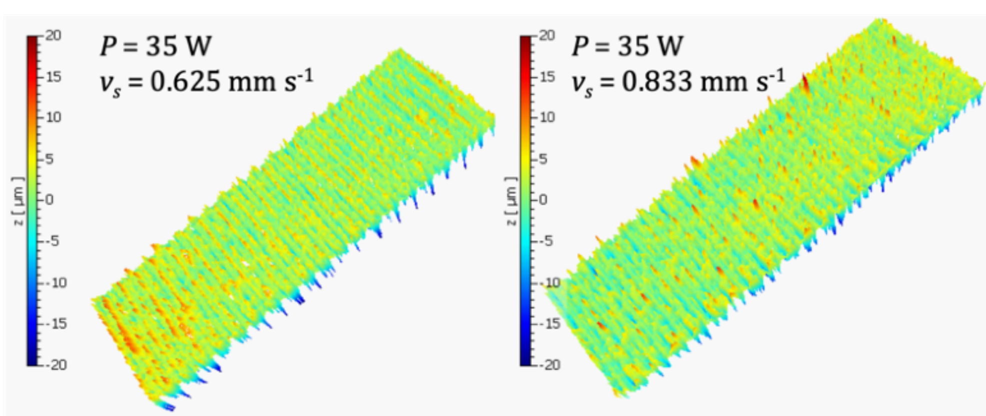

Figure 24. Surface areal texture height maps of the AISI D2 tool steel (single pass strategy).

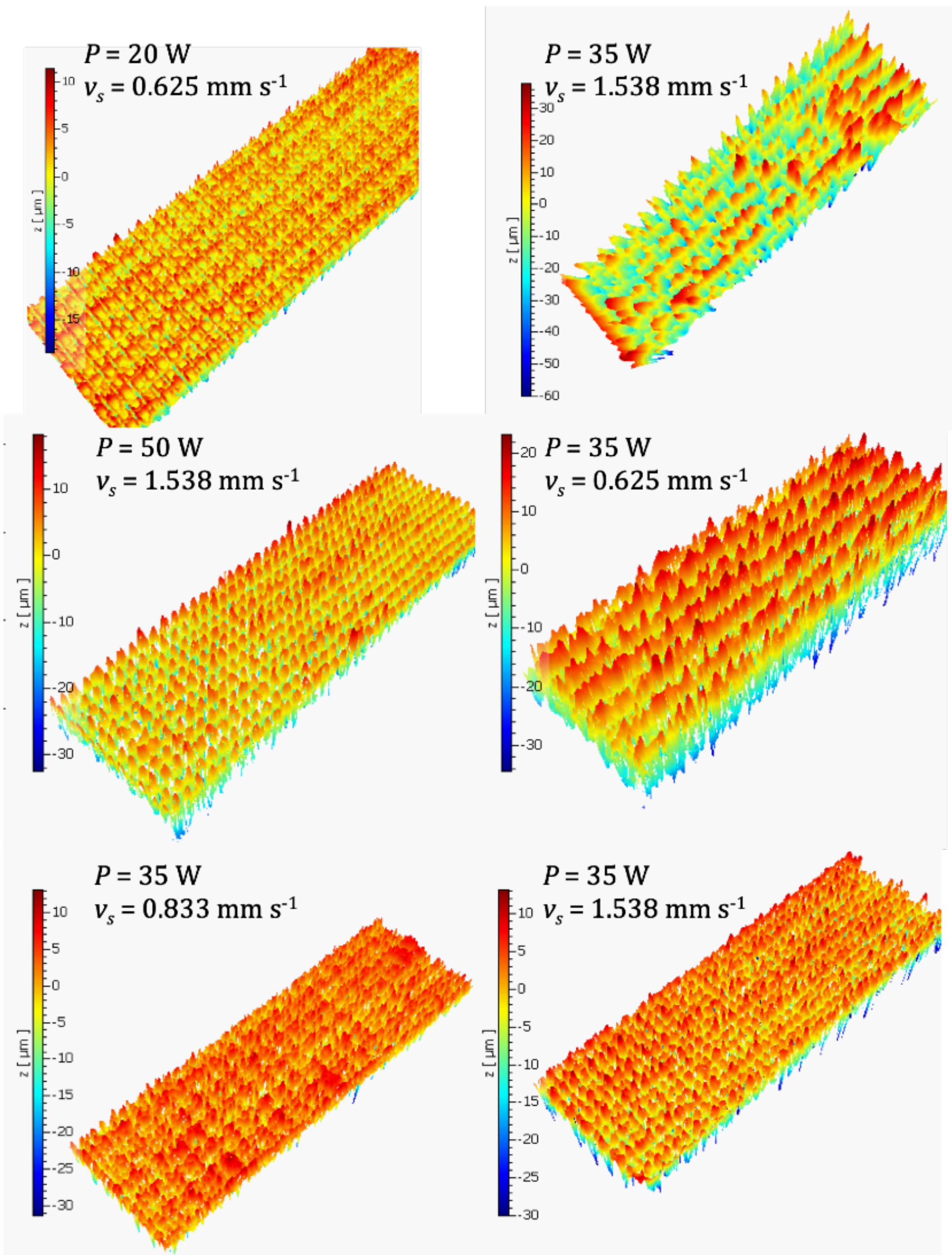

Figure 25. Surface areal texture height maps of the AISI D2 tool steel (double pass strategy).

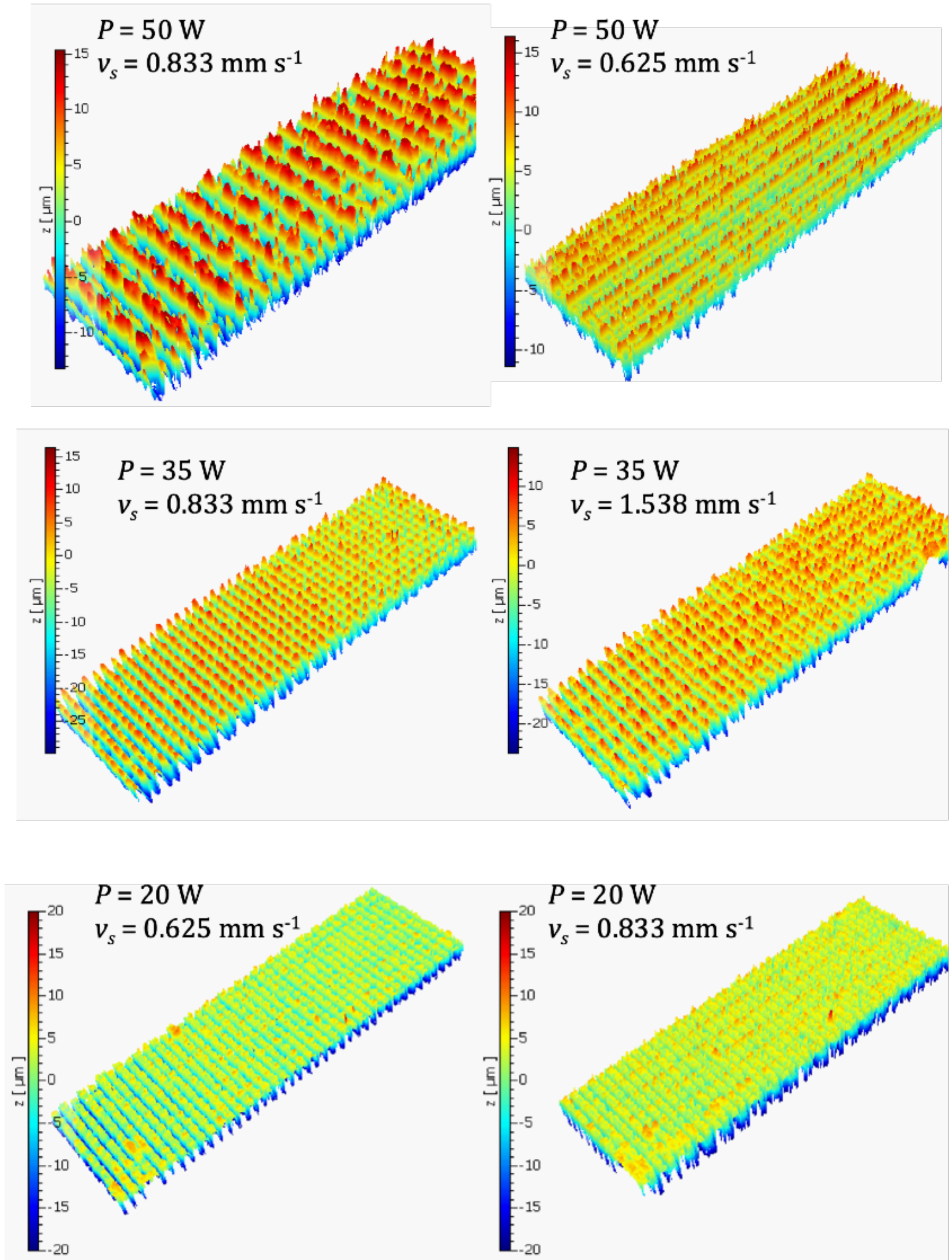

Figure 26. Surface areal texture height maps of the AISI D2 tool steel (triple pass strategy).

The measured values of the arithmetical mean height of the scale-limited surface *Sa*, the root mean square height of the scale-limited surface *Sq* (standard filtering conditions), and *Ssk* and *Sku*, skewness and kurtosis of the scale-limited surface are given in Table 5 for the single pass scan strategy with a pulse-to-pulse overlapping percentages between 99.95% and 99.99%.

Table 5. Surface texture parameters using single pass strategy.

P (W)	v_s (mm. s^{-1})	Trajectory	Sa (µm)	Sq (µm)	Sku	Ssk
50	0.625	Linear	2.74	3.28	0.59	2.93
50	0.833	Linear	8.27	9.60	-0.27	1.98
50	1.538	Linear	4.93	5.76	-0.14	2.00
35	0.625	Linear	2.25	3.10	-0.88	5.70
35	0.833	Linear	2.21	3.17	-1.25	9.41
35	1.538	Linear	2.43	2.74	0.34	2.17
20	0.625	Linear	1.76	2.26	0.23	3.83
20	0.833	Linear	3.13	4.03	-1.10	4.40
20	1.538	Linear	3.51	4.72	-1.46	-1.03

3.5 Effects of Process Parameters on Surface Texture

This analysis helped identifying effects of laser power and scan velocity on the measured texture line width, w_l, as shown in Fig. 27. It is observed that the line width of the parallel micro-texture ranges between little less than 0.200 mm and 0.220 mm with varying scan velocity from v_s = 0.625 mm. s^{-1} up to 1.538 mm. s^{-1}, and varying laser power from P = 20 W to 50 W. Increasing scan velocity lowers the texture line width and increasing laser power widens the line width, w_l, as expected. Hence, the combination as energy density can be used to control both effects of increasing laser power and increasing scan velocity.

Figure 8 shows the variation in texture line width as a function of laser power and scan velocity. Higher line width is preferred for the larger laser power and lower scan velocity. As can be seen from the figure, a non-linear variation of line width was found with increasing laser power and decreasing scan velocity which could also be illustrated by using energy density (the ratio between laser power and scan velocity). A line width of w_l = 0.2 mm and lower surface roughness was achieved with a laser power of P = 20 W.

A laser power greater than P =35 W and a scan velocity that is greater than 0.833 mm. s^{-1} produced a non-reasonable line width. Varying levels of power and scan velocity were also led to the similar results on the surface roughness (Sa, arithmetical mean height of the scale-limited surface). With the increase of scan velocity, the roughness decreased significantly while increased with the increase of laser power as shown in Fig. 28.

In order to achieve melting and vaporization, a threshold for plasma explosion is found to be 3 $GW.cm^{-2}$ or 20 $J.mm^{-2}$ for carbon steel [20]. The early stages of plasma ignited by surface electron emission action during nanosecond laser pulse processing.

In this study, the minimum laser fluence is $\Phi_{min} = 86.7\ J.mm^{-2}$ (P = 20 W, v_s = 1.538 mm. s^{-1}) that is higher than this threshold of plasma. This requires plasma shielding to improve the efficiency of the laser surface texturing since plasma plume absorbs incoming laser energy and reduces the ablation efficiency [20].

At *PRR*s up to 60 $\times 10^3$ s^{-1}, even though pulse overlapping is high, a low ablation efficiency occurs due to the synergetic effects of early-stage plasma shielding and thermal diffusion loss. The stronger plasma irradiation and molten droplets explosion result in chaotic ablated surface topography or molten metal accumulation at the edges of linewidth. It is shown that higher *PRR*s can stabilize this situation and the heat accumulation effect causes temperature approaching to or exceeding the carbon steel evaporation temperature, hence improving ablation efficiency. Consequently, combined effects of low ablation threshold, high heat accumulation and low plasma shielding could be accomplished in an acceptable range of *PRR* to improve ablation efficiencies and surface quality.

This illustrates the relationship between roughness and scan velocity/laser power for both double and triple passes scan strategies. They have the similar trend as the single pass has. A laser power higher than P =35 W produced significant surface roughness and a scan velocity higher than v_s = 0.833 $mm.s^{-1}$ resulted in better roughness when double pass strategy is employed. For the triple passes, it was found that the roughness decreased when the scan velocity and laser power increased.

Especially for the interaction effects between laser power and scan velocity on the surface roughness value (Sa), regardless of beam offset, increase in power deteriorates the surface finish, irrespective of the scan velocity. The reason is that laser power plays much more important role to the surface roughness than the scan velocity. The improvement in surface finish is attributed to repeated melting and thermal ablation, which effectively removed surface imperfections. A minimum surface roughness, Sa, of 2.19 μm or 4.2 μm was achieved when multiple passes such double and triple pass scan strategies are applied. It should be noted that the goal is not to achieve minimum surface roughness but a distinct texture with an acceptable texture line width.

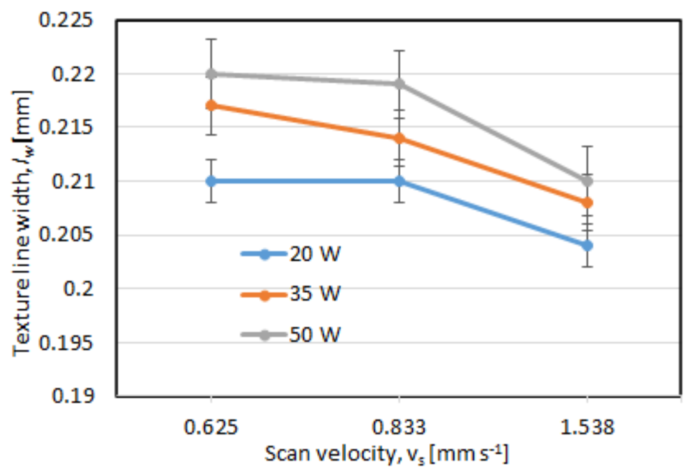

a)

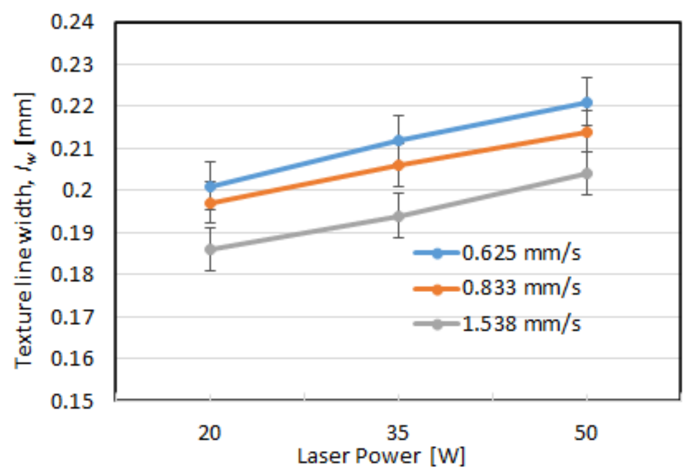

b)

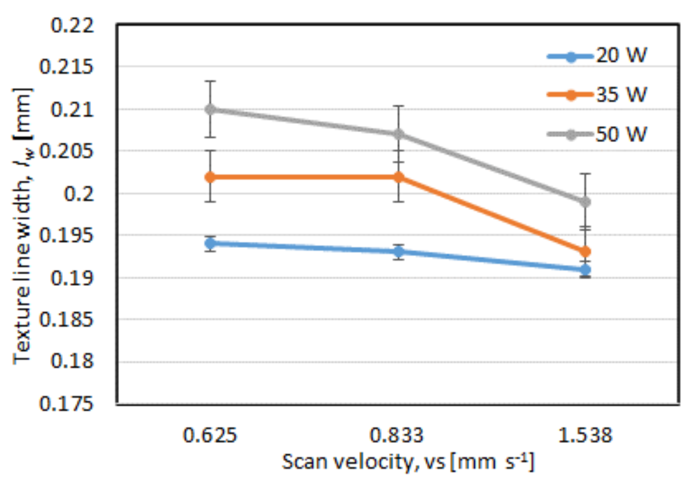

c)

Figure 27. The effect of laser power in a single pass strategy (a) and scan velocity in a double pass strategy (b) and triple pass strategy (c) on the line width of the parallel micro-textures.

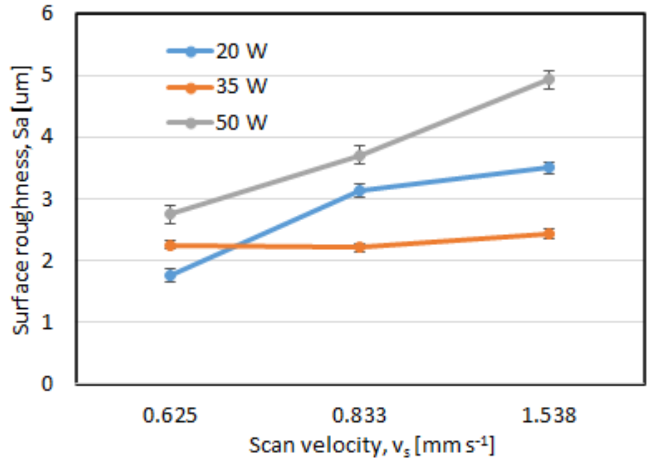

a)

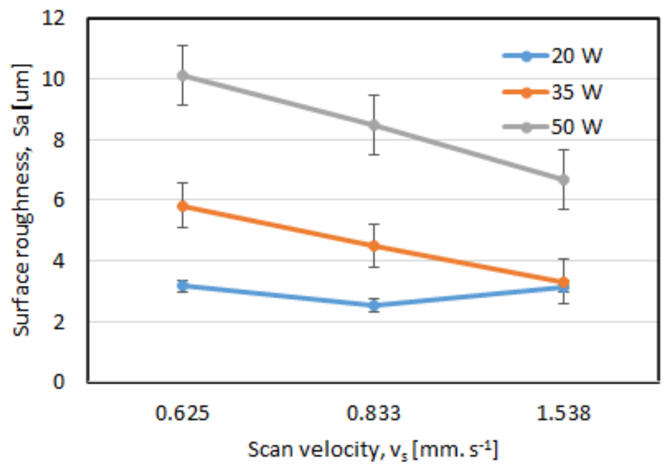

b)

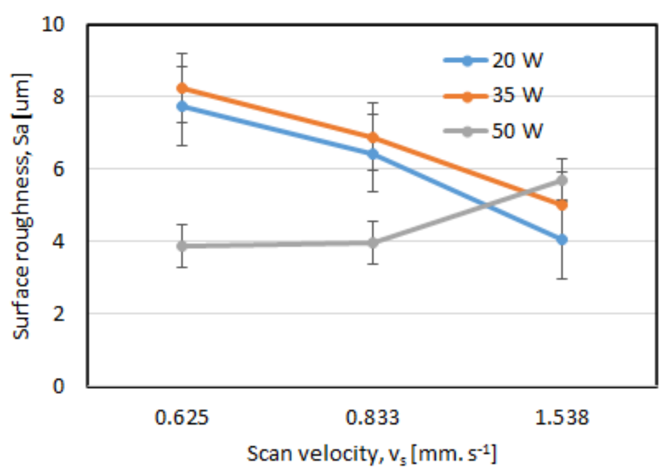

c)

Figure 28. The effect of laser power in a single pass strategy (a) and scan velocity in a double pass strategy (b) and triple pass strategy (c) on the surface roughness (Sa) on the surface of the parallel micro-textures.

From above results, the high laser power and slow scan velocity lead to wider texture line width whereas low laser power combined with fast scanning results in narrow texture line width. The line width increases with laser power and decreases with scan velocity while all other parameters are constant.

By combining laser power and scan velocity, the rise in laser energy density leads to rising in texture line width. The same trend is observed in all scan passes. The variation in texture line width with increasing energy density is represented with a regression model, which gives the texture line width value at a particular laser energy density as combination of laser power and scan velocity as embedded in Fig. 29.

Higher productivity (energy density) can be achieved with high scan velocity and low energy input (laser power). Laser power and scan velocity has significant control on the texture line width and its surface roughness during the laser surface texturing process.

From the above analysis, with increasing laser power, the line width increases correspondingly. With further increases in input energy, the surface condition starts to deteriorate. Similar effects were noticed when changing scan velocity for a constant laser power. At an optimal scan velocity, the striation patterns disappeared, and a uniform surface was achieved. Further increases in scan velocity resulted in small texture line width.

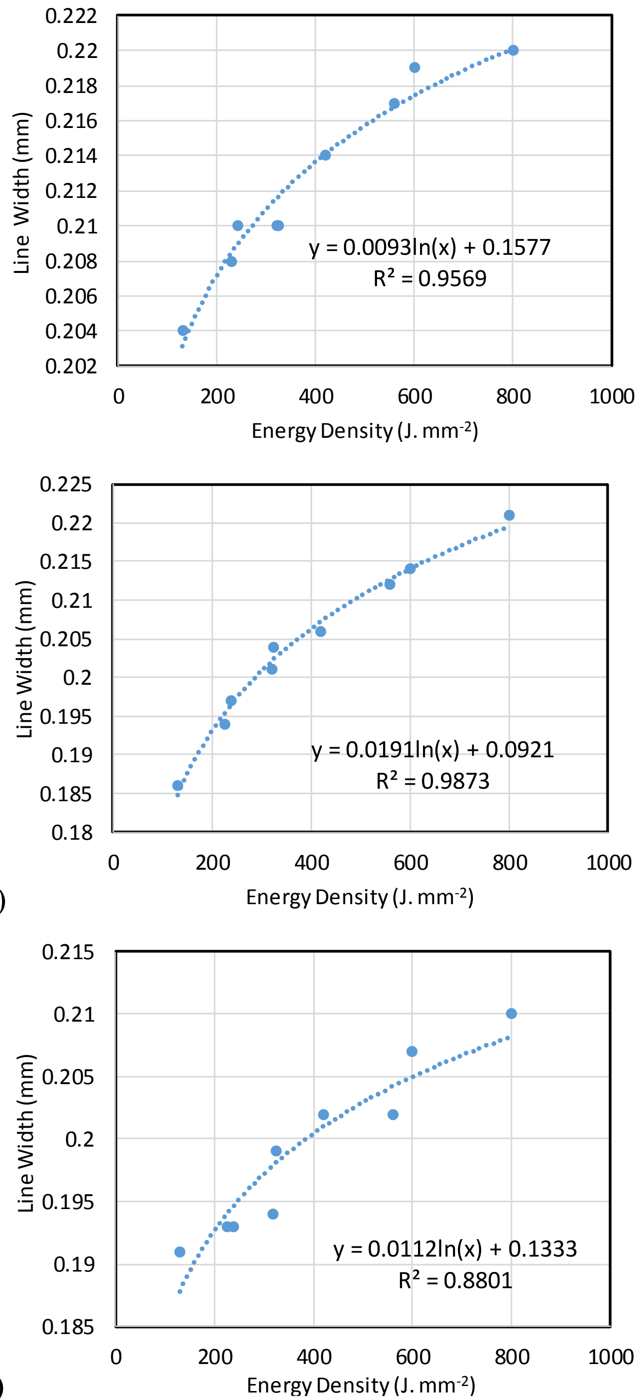

Figure 29. The effect of energy density on the line width of the parallel micro-textures in a single pass strategy (a) and scan velocity in a double pass strategy (b) and triple pass strategy (c). (R^2 represents the goodness of fit)

Chapter 4

Application of Machine Learning Methods

Machine learning is a form of artificial intelligence (AI) that enables a system to learn from data rather than through explicit programming. Machine learning methods are often utilized when trying to capture the process behavior by utilizing existing measured data. The methods involve either emulating the process behavior from the measured experimental data sets (artificial neural network) or using search method to search over a class of feasible solutions to find the optimal (generical programming) [25].

A machine learning model is the output generated when one trains an algorithm with measured data. After the training, one can use the predictive model that will provide an output with each given input. Machine learning techniques are required to improve the accuracy of predictive models. There are different approaches based on the type and volume of the data. Supervised learning typically begins with an established set of data and a certain understanding of how that data is classified. Supervised learning is intended to find patterns in data that can be applied to an analytics process. This data has labeled features that define the meaning of the data [25].

In this thesis study, based on the nature of the laser surface texturing data set, all of the processing parameters are categorized as labeled data, such as Sa, Sq, Ssk, Sku variables are used to identify surface texture parameters. Unsupervised learning is used when problem requires a massive amount of unlabeled data, such as social media applications.

In order to understand the logic behind imported data requires algorithms that classify the data based on the patterns or cluster it finds. Unsupervised learning conducts an iterative process, analyzing data without human intervention [25].

Artificial neural networks are one of the many tools used in machine learning. Neural networks are brain-inspired systems which are intended to replicate the way human brain learns. Neural networks consist of input and output layers along with multiple hidden layers that transform the input into something that output layer can use. They are useful tools for human programmer to extract and teach the machine to recognize patterns [26].

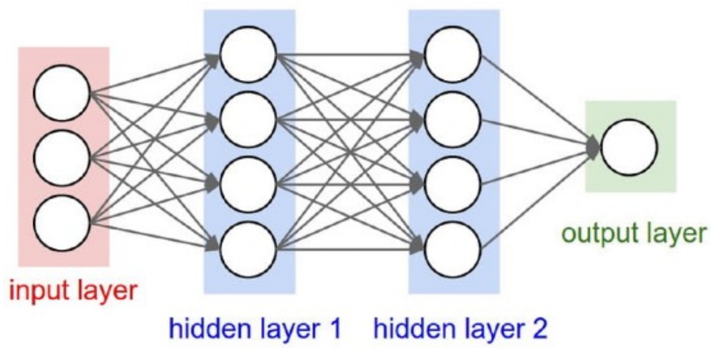

Figure 30. Artificial Neural Network Model (Multi-layer perceptron)

The principles of each layers can be easily explained by using the example of image processing. Input layer will be a picture of some object, first hidden layer will analyze the gray scale of each pixel in that photo, which tells the programmer the brightness of the object pixels. Then the second layer may identify edges of the image, by using edge descriptor base on lines of similar pixels. After this, another layer will gather the information from first two layers and recognize textures and shapes. Eventually the program goes through multiply layers like this and be able to distinguish certain image elements.

4.1 Artificial Neural Network Modeling Approach

A feedforward neural network is an artificial neural network wherein connections between the nodes do not form a cycle, its different from the descendant: recurrent neural network. Due to the nature of the problem, in this thesis the focus will be on feedforward neural network to generate a proper model to illustrate the relation between input parameters (laser power, scanning velocity, and energy density) and output which will surely be the surface texture parameters (Sa, Sq, Ssk, Sku) as shown in Fig.31.

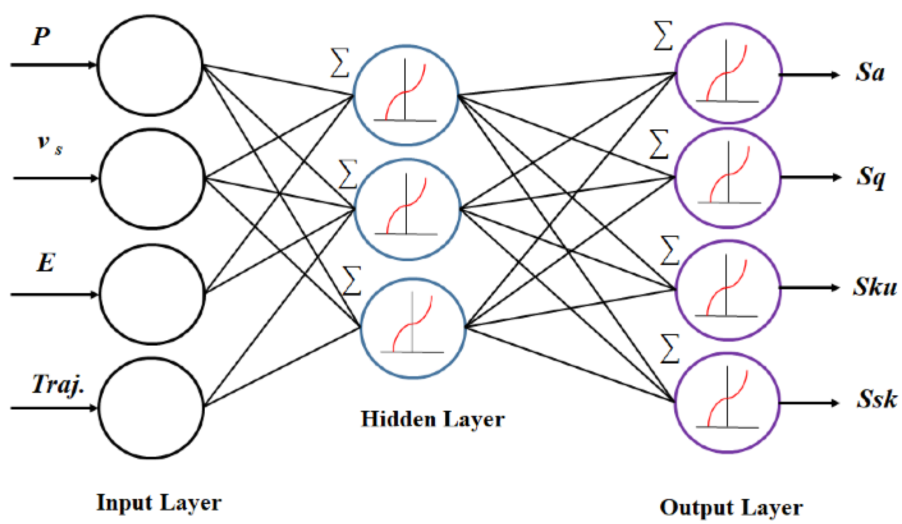

Figure 31. Model of a neural network algorithm for LST.

By utilizing feedforward neural network, one must understand which type of perceptron one needs to select. There are commonly two types of perceptron, single-layer perceptron or multi-layer perceptron. A single-layer perceptron network consists a single layer of output nodes, and the inputs are directly fed to the output through a series of weights. The sum of the products of the weights and the inputs is calculated in each node, and activation function will be applied on each neuron. The activation function will simply act like a "OR" logic, means if the value is above some threshold the neuron takes the activated value, usually 1, otherwise the deactivated value will usually be -1. Neurons with this kind of activation function are called linear threshold units, therefore we can draw the conclusion that single-layer perceptron is only a good fit for data which has linear relation.

Where the multi-layer perceptron usually interconnected in a feedforward way, each neuron in one layer has directed connections to the neurons of the subsequent layer, for this type of network, sigmoid functions is typically the activation function (other commonly used activation functions are *rectified linear unit* (ReLU) function and *tanh* function). Sigmoid function can alternate the value of each element from 0 to 1.

$$sigmoid(x) = \frac{1}{(1 + e^{-x})} \tag{5}$$

According to the chain rule, the derivative of sigmoid function will be:

$$sigmoid^{'}(x) = sigmoid(x)*(1 - sigmoid(x)) \tag{6}$$

The purpose of setting up hidden layer is achieve deep learning's rethinking generalization, in order to mimic some function which can represent the real world scenario. Any combination of two linear layer is not feasible to create non-linear relation, due to the fundamental theory of matrix operation, which is binary operators like multiplication or addition always generate an affine transformation between matrixes. The most obvious way in creating a non-linear network is applying activation function which is different from the "OR" logic that was stated earlier when discussing about single-layer perceptron, and "sigmoid function" is one of those different activation functions can be utilized to create non-linear network.

After choosing multi-layer perceptron network, backpropagation algorithm is utilized to train the feedforward neural networks for supervised learning [26].

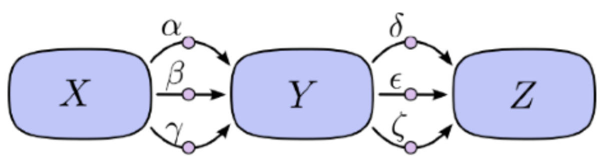

Figure 32. Model of a backpropagation algorithm

In fitting a neural network, backpropagation computes the gradient of the loss function with respect to the weights of the network for a single input-output example, this efficiency makes it feasible to use gradient methods for training multilayer network, updating weights to minimize loss; gradient descent, or variants such as stochastic gradient descent, are commonly used.

4.2 Predictive Artificial Neural Network Model by Using Backpropagation

In this section, the measurement data will be utilized in a multilayer perceptron (MLP) feedforward neural network approach that consists of three layers: input, hidden, and output layer to obtain relations between LST process parameters and surface texture parameters of the fabricated texture patterns on AISI D2 tool steel.

The inputs are laser power (*P*), scan velocity (v_s) and energy density (*E*). The outputs to be predicted are the surface texture parameters including arithmetic mean (Sa) and root-mean squared (Sq) heights of the scale limited surface and skewness (Ssk) and kurtosis (Sku) of the scale-limited surface are reported with the distinct effects of energy density and scan strategy on them.

Due to the design of experiment, and the process parameters tested are discrete values and it is not possible to adjust their values in a continuous manner, a binarized categorical treatment of process variables is a viable approach. In this sense, the process parameters can be treated as binary categorical variables instead of using their real values, and all process parameters do not have more than three levels. The measured values of surface texture parameters used in the predictive neural network modeling is given in Table 6. The categorial variables (x_1, x_2, x_3, x_4, x_5 are given in Table 7).

Table 6. The process input nominal value for surface texture measurement data used.

Data	*P* [W]	v_s [mm. s^{-1}]	*p* [mm]	*E* [J.mm^{-2}]	*Sa* [µm]	*Sq* [µm]	*Sku* [-]	*Ssk* [-]
1	50	0.625	0.40	200	2.74	3.28	0.59	2.93
2	50	0.833	0.40	150	8.27	9.60	-0.27	1.98

3	50	1.538	0.40	81	4.93	5.76	-0.14	2.00
4	35	0.625	0.40	140	2.25	3.10	-0.88	5.70
5	35	0.833	0.40	105	2.21	3.17	-1.25	9.41
6	35	1.538	0.40	57	2.43	2.74	0.34	2.17
7	20	0.625	0.40	80	1.76	2.26	0.23	3.83
8	20	0.833	0.40	60	3.13	4.03	-1.10	4.40
9	20	1.538	0.40	32	14.23	10.11	-1.46	-1.03

Table 7. The process input defined as binary values (True=1, False=0).

Data	x_1 (P =50W)	x_2 (P =35W)	x_3 (v_s =0.625 mm. s^{-1})	x_4 (v_s =0.833 mm. s^{-1})	x_5 (E =150 J.mm^{-2})	x_6 (E =50 J.mm^{-2})
1	1	0	1	0	1	0
2	1	0	1	0	1	0
3	1	0	1	0	1	0
4	0	1	0	1	0	1
5	0	1	0	1	0	1
6	0	1	0	1	0	1
7	0	0	0	0	0	0
8	0	0	0	0	0	0
9	0	0	0	0	0	0

The steps of the algorithm are given below, and it is run separately for each prediction output:

Step 1: The samples for training the network are prepared. In our study, the inputs are laser power, scan velocity and energy density, while the outputs are the arithmetic mean (Sa) and root-mean squared (Sq) heights of the scale limited surface and skewness (Ssk) and kurtosis (Sku) of the scale-limited surface.

Step 2: The initial parameters of the network are determined. Actually, those parameters could be changed according to the effects of training.

Step 3: The network weights and thresholds are initialized. The dimension of weight matrix $w_{ij}(t)$ is determined by the number of input factor and the number of neurons of hidden layer. The threshold is a critical value set to activate the neurons. Therefore, the number of thresholds is equal to the number of neurons based on the structure of the neural network.

Step 4: The input and output of the first layer of neurons are calculated. Assume that X is the input data. If the activation function of the first layer is linear function, the input and output of the first layer are equal to the values of the actual input data, $O_1 = X$. However, it is important to normalize the input and output samples since their dimensions and magnitudes are totally different.

Step 5: The input of the second layer of neurons are calculated. For the second layer, the input of neurons I_2 must be the sum of the values of all neurons in the first layer and threshold, $I_2 = w_{ij} \times X + B_{ij} \times ones$, where $ones$ is an array of all ones.

Step 6: The output of the second layer of neurons are calculated. If the activation function of the second layer is sigmoid function, $f(x) = \dfrac{1}{1+e^{-x}}$, the output of the second layer is $O_2 = \dfrac{1}{1+e^{-I_2}}$.

Step 7: The input and output of the third layer are calculated. Similar with the second layer, the input of third layer is $I_3 = w_{jk} \times O_2 + B_{jk} \times ones$. Since the activation function of the third layer is linear function, the output of the third layer is $O_3 = I_3$.

Step 8: The energy function *E* is calculated. The purpose of calculating the energy function is to stop training the network when the predetermined error is reached. According to the definition of energy function,

$$E = \sum (Y - O_3)^2 \tag{7}$$

where Y is the actual output.

Step 9: The adjustments of weight and threshold between the second and third layers are calculated. Hence,

$$\Delta\, w_{jk} = -\,\eta \frac{\partial E}{\partial w_{jk}} = -\,\eta \times (Y - O_3) \times O_2 \tag{8}$$

$$\Delta\, B_{jk} = -\,\eta \frac{\partial E}{\partial B_{jk}} = -\,\eta \times (Y - O_3) \times ones \tag{9}$$

Step 10: The adjustments of weight and threshold between the first layer and the second layer are calculated. Calculate the weight and threshold adjustment between the second and third layer before calculating those adjustments between the first and second layer. Therefore,

$$\Delta w_{ij} = -\eta \frac{\partial E}{\partial w_{ij}} = -\eta \times w_{jk} \times (Y - O_3) \times O_2 \times (1 - O_2) \times X \tag{10}$$

$$\Delta B_{ij} = -\eta \frac{\partial E}{\partial B_{ij}} = -\eta \times w_{jk} \times (Y - O_3) \times O_2 \times (1 - O_2) \times ones \tag{11}$$

Step 11: The weight and threshold after adjustment are calculated. The weights and thresholds at time $t+1$ are equal to the sum of them at time t and adjustments. The equations are listed as follows,

$$w_{jk}(t+1) = -\eta \frac{\partial E}{\partial w_{jk}} + w_{jk}(t) = \Delta w_{jk} + w_{jk}(t) \tag{12}$$

$$B_{jk}(t+1) = -\eta \frac{\partial E}{\partial B_{jk}} + B_{jk}(t) = \Delta B_{jk} + B_{jk}(t) \tag{13}$$

$$w_{jk}(t+1) = -\eta \frac{\partial E}{\partial w_{ij}} + w_{ij}(t) = \Delta w_{ij} + w_{ij}(t) \tag{14}$$

$$B_{ij}(t+1) = -\eta \frac{\partial E}{\partial B_{ij}} + B_{ij}(t) = \Delta B_{ij} + B_{ij}(t) \tag{15}$$

Step 12: The network output values are restored. Because the input and output are normalized for training the network, the O_3 needs to be denormalized to ordinary data.

Both categorical values (Table 7) and nominal values (Table 6) are implemented into the same ANN model and trained by strictly following steps presented above. The results are compared in terms of two performance metrics: i.e., Mean Square Error (MSE) and Mean Absolute Percentage Error (MAPE),

$$MSE = \sum_{i=1}^{6} (y_i - \hat{y}_i)^2 / n \tag{16}$$

$$MAPE = \sum_{i=1}^{6} \left| y_i - \hat{y}_i \right| / n \tag{17}$$

where; y_i is the actual value of the i^{th} data point and $\hat{y}_i$ is the predicted value of the i^{th} data point. From Table 8, it is obvious that ANN model adopting nominal values has much better performance than categorical. The nominal values implemented model has smaller Mean Square Error (MSE) and Mean Absolute Percentage Error (MAPE).

Table 8. Results of categorical and nominal values for predicting the surface texture parameters.

	Catagorical Values		Nominal Values	
	MSE	MAPE	MSE	MAPE
Sa	0.5485	6.6383	2.99E-05	1.51E-09
Sq	0.3432	3.1102	2.73E-04	1.59E-07
Ssk	0.9017	0.2149	1.67E-05	1.72E-10
Sku	0.3512	1.5299	1.72E-04	3.20E-10

The predictive ANN model is used against the measured data as shown in Fig. 33. The measured and predicted surface texture/ roughness parameters using the ANN model at varying energy levels (no rotations for a single line trajectory) are shown for Sa, Sq, Sku, Ssk.

These figures indicate the goodness of computations when ANN are utilized with the full test data set utilized as training set in surface texture measurements in LST. However, if one of the test conditions is removed from the training set, the computations are found to be not so good. This means that there should be more measurement data needed to improve the ANN model computations. Especially ANNs tend to overfit the model to the data in the absence of sufficient data; hence, with inclusion of more measurement data, the ANN model is expected to reflect the actual conditions.

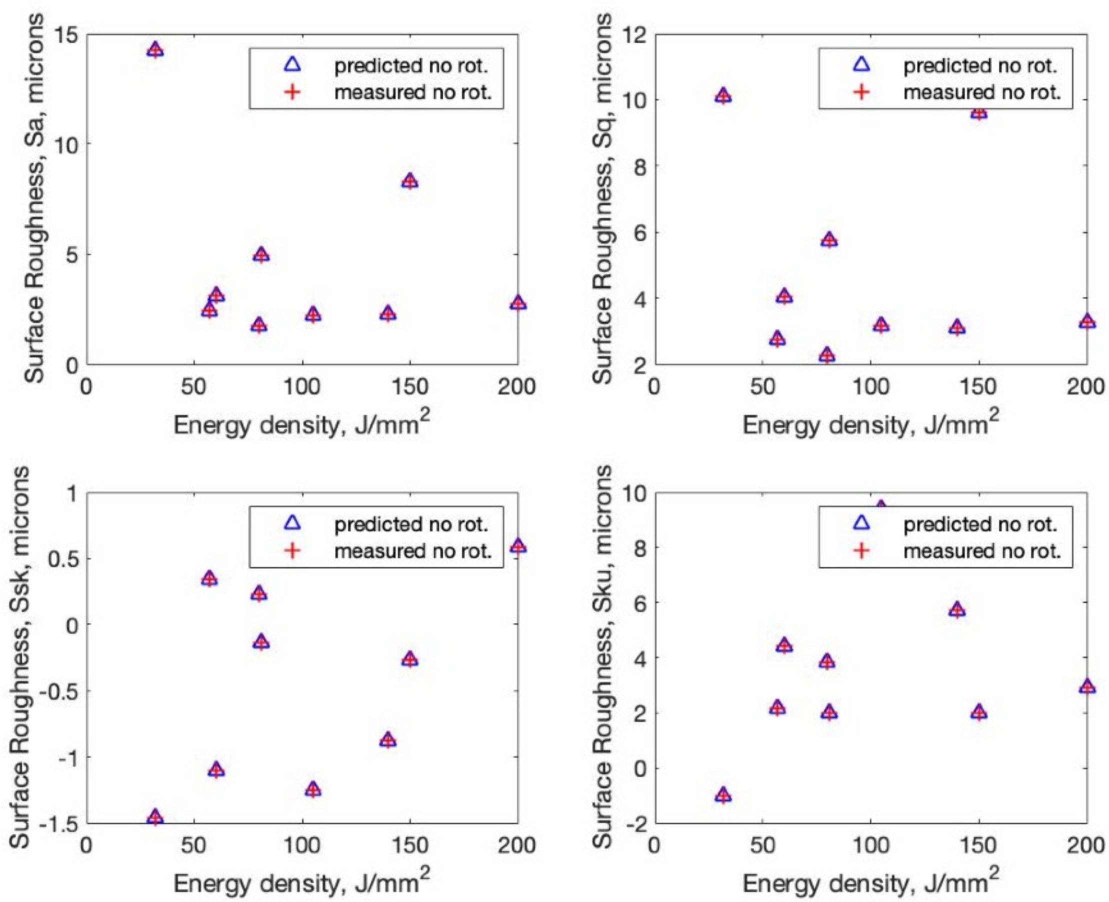

Figure 33. BP feedforward ANN model for predicting surface texture parameters.

Chapter 5

Conclusions and Future Work

This thesis study investigates the laser surface texturing (LST) process. In particular, the thesis focuses on effect of laser processing parameters such as laser power, scan velocity, on fabricating parallel textures with desired surface texture parameters. By applying multiple passes of parallel trajectories during the laser surface texturing process, it was possible to significantly reduce the measured surface texture parameters such as average surface roughness.

Furthermore, a regression relationship between laser energy density and surface texture parameters are defined so that these can be used for process planning purposes in laser surface texturing.

Surface topography investigations of laser textured surfaces were performed by obtaining areal height maps using white light interferometry technique for tool steel samples processed at various laser energy density settings and three different scan strategies, i.e. single, double, and triple passes.

Surface areal height maps showed the highly irregular surface texture created by laser surface texturing at low scan velocities and high energy densities due to chaotic laser ablation. Effects of laser surface texturing process parameters on the surface texture and roughness parameters have been identified.

Machine learning methods with neural networks were applied to the measured surface texture data to determine input and output relationships between LST process parameters and measured surface texture parameters with good predictive capabilities.

Some specific conclusions on the LST process can be drawn from this study include:

i) Micro-pattern produced on the surface of tool steel is sensitive to laser energy density as well as laser power, scan velocity, and pulse repetition rate.

ii) The combined effects of low ablation threshold, high heat accumulation, and low plasma shielding could be accomplished in an acceptable range of pulse repetition rate to improve ablation efficiencies and surface quality.

iii) An inefficient ablation can occur because of early-stage plasma shielding and thermal diffusion loss when high overlapping is employed.

iv) A chaotic ablated surface topography or molten metal accumulation can be seen due to plasma irradiation and molten droplets explosion.

The advantages of employing such predictive models for laser surface texturing is the highlight of this thesis research. The future work is recommended on the following topics for further investigations.

i) There is an improvement needed in replacing positioning stages with step motor drives with a precision scan head instrument based on fast scanning galvanometers for x-axis and y-axis motions and a finer focus optics for the laser beam

ii) There is a need to develop in-situ process monitoring system to view the laser processes area using optical or thermal camera imaging systems.

iii) There is also more data needed to construct and develop a fully competent predictive modelling system that can predict the surface texture and roughness more accurately.

iv) Other methods of machine learning such as deep learning methods should be studied for more established predictive artificial intelligence capability for the machine tool.

References

[1] ISO 25178-2 B.E. (2012), BS EN ISO 25178-2, in Geometrical product specifications (GPS) Surface texture: Areal 2: Terms, definitions and surface texture parameters. British Standards Institute.

[2] Ibatan, T., Uddin, M.S., & Chowdhury, M.A.K. (2015) Recent development on surface texturing in enhancing tribological performance of bearing sliders. *Surface and Coatings Technology*, *272*, 102-120.

[3] Wang, Z., Hu, S., Zhang, H., Ji, H., Yang, J., & Liang, W. (2018) Effect of surface texturing parameters on the lubrication characteristics of an axial piston pump valve plate. *Lubricants*, *6* (2), 49.

[4] Hamilton, D.B., Walowit, J.A., & Allen, C.M., 1966, A theory of lubrication by microasperities, *ASME J. Basic Eng*., *88*(1), 177–185.

[5] Anno, J.N., Walowit, J.A., & Allen, C.M. (1968) Microasperity lubrication, *ASME J. Lubr. Technol*., 90 (2), pp. 351–355.

[6] Anno, J.N., Walowit, J.A., & Allen, C.M. (1969) Load support and leakage from microasperity-lubricated face seals, *ASME J. Lubr. Technol*., *91*(4), 726–731.

[7] Etsion, I. (2005) State of the art in laser surface texturing. *J. Trib*., *127*(1), 248-253.

[8] Šugár, P., Šugárová, J. & Frnčík, M. (2016) Laser surface texturing of tool steel: textured surfaces quality evaluation. *Open Engineering 6*:90-97.

[9] Tanga, W., Zhoua, Y., Zhua, H., Yanga, H. (2013) The effect of surface texturing on reducing the friction and wear of steel under lubricated sliding contact. *Applied Surface Science 273*: 199–204.

[10] Putignano, C., Scaratia, D., Gaudiusob, C., Mundod, R., Anconab, A., Carbonea, G. (2019) Soft matter laser micro-texturing for friction reduction: An experimental investigation. *Tribology International 136*: 82–86.

[11] Cunha, A., Elie, A.M., Plawinski, L., Serro, A.P., Botelho Do Rego, A.M., Almeida A, et al. (2016) Femtosecond laser surface texturing of titanium as a method to reduce the adhesion of Staphylococcus aureus and biofilm formation, *Applied Surface Science 360*: 485–493.

[12] Mencia, G., Demir, A.G., Waugh, D.G., Lawrence, J., Previtali, B. (2019) Laser surface texturing of β-Ti alloy for orthopaedics: Effect of different wavelengths and pulse durations. *Applied Surface Science 489*: 175–186.

[13] Chun, D.M., Ngo, C.V., & Lee, K.M. (2016) Fast fabrication of superhydrophobic metallic surface using nanosecond laser texturing and low-temperature annealing. *CIRP Annals*, *65*(1), 519-522.

[14] Silva, W.M.D., Suarez, M.P., Machado, A.R., Costa, H.L. (2013) Effect of laser surface modification on the micro-abrasive wear resistance of coated cemented carbide tools. *Wear 302*: 1230–1240.

[15] Xing, Y.Q., Deng, J.X., Wang, X.S., Ehmann, K., Cao, J. (2016) Experimental assessment of laser textured cutting tools in dry cutting of aluminum alloys. *Journal of Manufacturing Science and Engineering 138*: 071006.

[16] Sugihara, T., Toshiyuki, E. (2017) Performance of cutting tools with dimple textured surfaces: a comparative study of different texture patterns. *Precision Engineering 49*: 52–60.

[17] Sugihara, T., Nishimoto, Y., Enomoto, T. (2017) Development of a novel cubic boron nitride cutting tool with a textured flank face for high-speed machining of Inconel 718. *Precision Engineering 48*:75-82.

[18] Su, Y., Li, Z., Li, L., Wang, J., Gao, H., Wang, G. (2017) Cutting performance of micro-textured polycrystalline diamond tool in dry cutting. *Journal of Manufacturing Processes 27*: 1-7.

[19] Niketh, S., & Samuel, G. L. (2017) Surface texturing for tribology enhancement and its application on drill tool for the sustainable machining of titanium alloy. *Journal of Cleaner Production*, *167*: 253-270.

[20] Wu, B., Deng, L., Liu, P., Zhang, F., Duan, J., Zeng, X. (2017) Effect of picosecond laser repetition rate on ablation of Cr12MoV cold work mold steel. *Applied Surface Science. 409*:403-412.

[21] Ahuir-Torres, J.I, Arenas, M.A., Perrie, W., de Damborene, J. (2018) Influence of laser parameters in surface texturing of Ti6Al4V and AA2024-T3 alloys. *Optics and Lasers in Engineering 103*: 100–109.

[22] TopMap Pro.Surf.（2019）Optical surface metrology, for quality control applications, Datasheet, Polytec GmbH, Waldbronn, Germany.

[23] ISO 25178-3 B.E.（2012）in Geometrical product specifications (GPS) Surface texture: Areal Part 3: Specification operators. British Standards Institute.

[24] ISO 25178-2 B.E.（2012） in Geometrical product specifications (GPS) Surface texture: Areal 2: Terms, definitions and surface texture parameters. British Standards Institute.

[25] Hastie, T., Tibshirani, R., Friedman, J. (2017) *The Elements of Statistical Learning Second Edition*, Springer Science & Business Media, New York, NY, USA.

[26] Goodfellow, I., Bengio, Y., Courville, A. (2016) *Deep Learning*, MIT Press, Cambridge, MA, USA.